Publications of the Institute of Geophysics, Polish Academy of Sciences
Geophysical Data Bases, Processing and Instrumentation
vol. 442 (D-77), 2022, pp. 85–119
DOI: 10.25171/InstGeoph_PAS_Publs-2022-027

A Novel Application of the Virtual Fujita Scale (VFS) Number Approach as a Useful Tool for Assessment of Lightning Discharges Development and Severity for the Derecho Episode in Poland on 11 August 2017 Together with its Synoptic Context

Jan PARFINIEWICZ[1*,✉], Piotr BARAŃSKI[2,✉], and Michał HERMANOWICZ[3,✉]

[1]Institute of Meteorology and Water Management – National Research Institute, Warsaw, Poland

[2]Institute of Geophysics, Polish Academy of Sciences, Warsaw, Poland

[3]Interdisciplinary Centre for Mathematical and Computational Modelling (ICM), University of Warsaw (UW), Warsaw, Poland

*retired

✉ Jan.Parfiniewicz@gmail.com
✉ baranski@igf.edu.pl
✉ m.hermanowicz@icm.edu.pl

A b s t r a c t

Everyone agrees that the episode of the derecho of 11 August 2017, commonly known as "Suszek", was the most catastrophic weather event in Poland of the last decade. This case of a rapidly and very fast-moving mesoscale convection system (MCS) is still being analyzed. The current work uses the lightning detection data from the PERUN remote sensing system, which allowed to estimate the electrical activity of such a huge convection system. The primary lightning discharge density is then transformed into the useful scalar parameter, i.e., the predictor characterizing lightning and convection severity of the considered MCS and denoted farther as the virtual Fujita scale (VFS) number. The scrutinized analysis conducted by us presents firstly the detailed mapping of disturbance involved in the MCS propagation path by using the moving filters approach, secondly the area determination of the MCS event development in the form of a mask, and thirdly the analysis of selected aspects of the phenomenology of the MCS occurrence. Such filters make it possible to split the main space domain of the considered convection area into two separated parts of each filter, i.e., its west and east flanks/sides.

A refined analysis and comparison of the aside thunderstorm tracks allowed us to better characterize the development structure of the considered MCS region. In this case, the meteorological context of the MCS episode, i.e., the influence of synoptic background on the course of such a convection, was essential. A better understanding of this violent convective process requires a detailed and complex diagnosis of the complementary and additional information coming from various measurement and database sources, e.g., the ground meteorological measurements, lightning discharges detections and locations, radar and satellite observations together with the relevant model simulations and various severe weather reports. In turn, the used data should be projected/presented in the common and one reference grid. This common reference context was provided by the operational computer simulations at 12:00 and 18:00 GMT of the derecho day expressed by the study of the 3D fields of such parameters as the air pressure, the potential temperature of the tropopause, the air vorticity, the vertical component of air motion and the turbulence air potential. This last was broken down into two components related to the Reynolds and Richardson numbers. The first component represents momentum and is denoted further as PT_{Re} and the second one, relevant to buoyancy and the air flow shear, is denoted by PT_{Ri}. The presented approach allowed for a rational tracking of the evolution of the whole MCS system connected with the derecho episode in Poland.

Keywords: derecho, convection, mesoscale convection system, propagation path, movable filter, lightning location system.

1. INTRODUCTION

Celiński-Mysław and Matuszko (2014) reported and analyzed six cases of the derecho phenomenon that occurred in Poland in 2007–2012. They have found that the regions that were most often affected by the derechos lay in southern and central Poland, but the derecho of "Suszek", that occurred between 12:40–23:50 UTC on 11 August 2017 and propagated along the SW-NE line was the most disastrous in the last decade, as noted by Taszarek et al. (2019a,b). Among the 6 victims, there were also two girl scouts who died near the site of Suszek, and the case had a court epilogue. During the 10-th European Conference on Severe Storms – ECSS in Kraków, Poland, on 4–8 November 2019, there were at least three poster presentations given by Taszarek et al. (2019a,b), Mazur et al. (2019), and Barański and Parfiniewicz (2019), devoted to the comprehensive analysis of time and space development of different meteorological sources of the "Suszek" derecho incident. This case of a violently and very fast-moving MCS, as shown in the satellite data by Łapeta et al. (2021), is very different from the cases of tornadoes generated by classical, large and slowly moving supercells, reported previously by Parfiniewicz and Barański (2014). Here, the structure of the jet stream, located above the western border of Poland was crucial for supporting the convective system and moving it to the northeast, as was indicated by Taszarek et al. (2019a,b), Mańczak et al. (2021), and Wrona et al. (2022).

In the works mentioned above, the lightning activity of the MCS was not considered at all; therefore, it was advisable to address this issue of lightning activity with greater detail. The operational system of lightning discharge detections PERUN was active during the MCS life time and the PERUN lightning data have supplemented perfectly the radar reflectivity scans of the considered convective system. The detected lightning discharge zones are more compact objects compared to the radar scans of the vast and huge MCS. Hence, such lightning discharge zones may be considered as a kind of compact signature that is more convenient to monitor the MCS's time and space development. The subject of the presented work was to collect and analyze the data of lightning discharge detections that were gathered during the derecho catastrophic event on 11 August 2017. The carried analysis converts the lightning discharge detections to the so-called virtual Fujita scale (VFS) number. The area changes of the particular

VFS number were used to determine the considered MCS propagation path, its duration and distance traveled, and additionally to indicate also its path split time moment together with this split location.

2. USING OF THE PERUN LIGHTNING DETECTION DATA TO INTRODUCE THE USEFUL SCALAR PARAMETER DENOTED THE SEVERITY DEGREE GENERATED BY MCS EVENTS

PERUN is the Polish name of the French lightning detection and location system called SAFIR (in French: Surveillance et Alerte Foundre par Interférométrie Radioélectrique) that has operated in Poland since 2002. This system enables one to detect and locate atmospheric discharges using the interferometry techniques in the VHF frequency band (Richard and Lojou 1996). Additionally, the low-frequency electromagnetic waves generated by lightning discharges are also analyzed to measure some electrical parameters of these discharges and to discriminate between their types. Such a system mainly uses the arrival signal direction finding (DF) technique to determine the plane locations of lightning sources by the geographical coordinate and distinguishes three groups of detected lightning incidents: the cloud-to-ground flashes by their positive or negative strokes, the intra-cloud lightning discharges by their nodes and the so-called isolated points, i.e., not fully discriminated the flash strokes (Bodzak et al. 2006; Parfiniewicz 2013).

The data from PERUN lightning detection and localization system are transformed into a useful scalar parameter that is characterizing the severity of MCSs or other Extreme Convective Phenomena (ECP). Such a parameter is called Virtual Fujita Scale (VFS) and is similar to some extent to the original Fujita scale (F) postulated by Fujita (1978). On the other hand, Parfiniewicz (2012) proposed some new empirical formulas that enable to transform the primary lightning discharges density field to the relevant VFS parameter/number. Such transformation was based on and validated by the statistical correlation between the occurrence of the severe weather events evaluated in the primary Fujita scale (F) by the SKYWARN POLSKA database and the frequency occurrence of IC (intracloud) or CG (cloud-to-ground) lightning discharges detected and located by the PERUN system and archived in its database. Due to that, two statistical formulas, i. e., F_a and F_b, as a function of lightning discharge densities have been proposed.

The best-fitted formula for the cases of strong ECP events, with the number of lightning discharges (NoL) under the condition that there is at least one return stroke (RS) detection of CG flash and the whole IC lightning discharge detection consists of more than 70 node signals separated in time, is then given by Eq. (1):

$$F_a = a \times (b \times \mathrm{ICs} + c \times \mathrm{ICi})^{1/2} + d \ , \tag{1}$$

where: $a = 0.047$, $b = 0.7$, $c = 0.3$, $d = 0.22$, and ICs, ICi are measured/expressed in the units $(\mathrm{NoL}/\pi \times (15\ \mathrm{km})^2 \times 10\ \mathrm{min})$. Here ICs denote the number of the first inter-cloud discharge node signals detected by the PERUN as the starting lightning source emission points. ICi is the burst of intermediate lightning emission points showing the whole IC flash event development in 2D.

For less severe convective events, i.e., with $0 < F \leq 2.5$, another formula, that includes both CG (with the number of RS > 1) and IC lightning flash detection data given by ICs number, is expressed by Eq. (2):

$$F_b = a \times [b \times \mathrm{ICs} + c \times \mathrm{RS} + d \times (\mathrm{ICs} \times \mathrm{RS})^{1/2}]^{1/2} \ , \tag{2}$$

where: $a = 0.088$, $b = 0.624$, $c = 0.112$, $d = 0.264$.

Basing on the calculated value of F_a and F_b, and taking into account the above-mentioned limitations, the resulting convective strength of the considered MCS event is finally evaluated as $[F_0]$ = maximum (F_a, F_b).

This conversion of PERUN lightning detection data was carried out on 7 km × 7 km and 2.8 km × 2.8 km grids, but for each grid mode, any lightning detection points are attributed to their circle surroundings with a radius up to 15 km. It means that, if any PERUN lightning detection points are found in such an area, then the value of lightning discharge density at this site accounts for the number of all lightning discharge locations detected in the circle of 15 km radius surrounding the primary cell of the chosen grid net.

It is worth noting that the relationship between the calculated VFS number and the number of ICs, ICi, and RS obtained from the considered PERUN lightning detection data for the selected VFS threshold level in the range from 1 to 5, depends generally on the used grid model resolution and noted lightning statistics. Here, for the used COSMO (COnsortium for Small-scale MOdeling) _07 km reference grid model and taking into account 10-minute intervals for PERUN lightning detection data during the whole day of 11 August 2017, our exemplary VFS threshold calculations are summarized in Table 1.

Table 1

Relationship between ICs, ICi, and RS number obtained from the PERUN lightning detection data in 10-minute intervals and with the used COSMO_07 km reference grid model, and related to the selected VFS number threshold in the range from 1 to 5

PERUN detection of ICs incidents	PERUN detection of ICi incidents	PERUN detection of RS incidents	Range of VFS number threshold
139.	117.	78.	1.0
636.	361.	233.	2.0
1514.	1036.	347.	3.0
2652.	2073.	590.	4.0
4128.	2839.	1090.	5.0

Such formulas, Eqs. (1)–(2), were also used by Barański and Parfiniewicz (2019) to create a nowcast prediction of severe thunderstorm occurrence connected with the derecho episode in the Bory Tucholskie district on 11 August 2017. This approach was tested in real time by the weather forecasters. It is worth noting that the presented method in this section allowed for efficient and reliable identification of different types of severe convective events, including also tornado incidents.

3. THREE CONVECTIVITY DEVELOPMENT STAGES OF THE DAY WITH THE DERECHO EPISODE

The convective activity of the whole day of 11 August 2017, represented by the density of lightning discharges, is at first divided into three development stages. The analysis, based on Eqs. (1)–(2) given in the previous section, uses 144 patterns of the Virtual Fujita Scale (VFS) number field obtained from the PERUN lightning detection data and recalculated in every 10-minute intervals. By scrolling through them and animating these scans, it is possible to identify these changes that are characteristic of each development stage of the considered MCS. Each of the 3 subjectively identified stages was described by the summary maps of the maximum values of a given parameter that occurred at the given position during that stage. Hence, such maps present electrical activity (EA) expressed by the calculated relevant VFS number and

overlapped on the radar reflectivity and the radar-derived precipitation. The radar-derived precipitation was calculated according to the INCA system reported by Szturc et al. (2018) and using the "radar precipitation" formula given by Marshall and Palmer (1948). Thus, such radar-derived precipitation is similar to the primary radar reflectivity data.

Finally, we have divided the considered MCS development from 11 August 2017 into three different phases. The first started before 04:40 UTC and was evaluated as a very strong thunderstorm convection preceding the derecho event. The second lasted from 04:50 to 12:30 UTC and was determined as the intermediate period with two separated thunderstorm episodes and the third one lasted from 12:40 to 23:50 UTC and was connected with the catastrophic gust wind incidents of violent convection that swept over Poland. These differentiated stages are presented in Figs. 1–3, respectively. Let us note, after Mańczak et al.

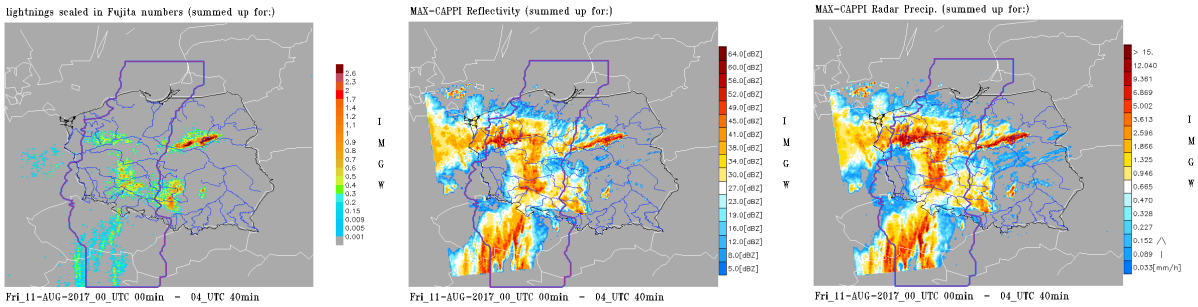

Fig. 1. Three signature maps presenting the first development stage of the considered MCS in the time interval from 00:00 to 04:40 UTC on 11 August 201 by electric activity expressed through fields of VFS number, radar reflectivity, and radar precipitation parameters, respectively, from left to right. The area denoted by the violet line shows the used mask to report/analyze the propagation path of the main MCS part/core during the whole day of 11 August 2017.

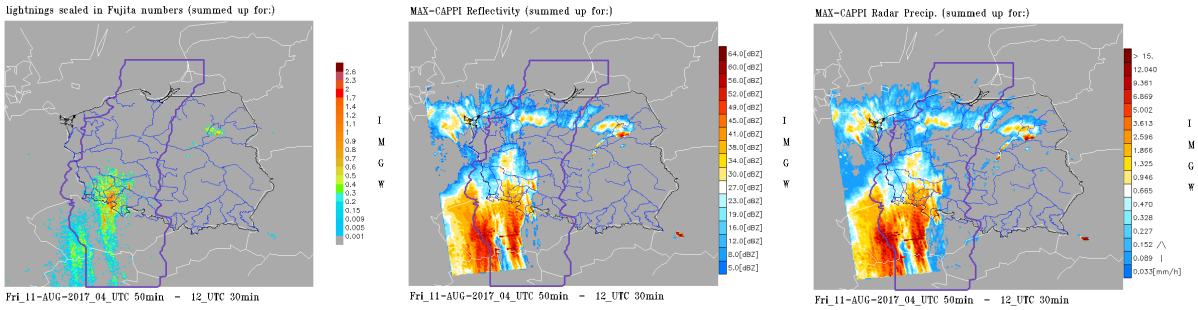

Fig. 2. The same as in Fig. 1, but for the time interval from 04:50 to 12:30 UTC on 11 August 2017, representing the second development stage of the considered MCS with the relevant three signature maps showing the intermediate and moderate thunderstorm activity.

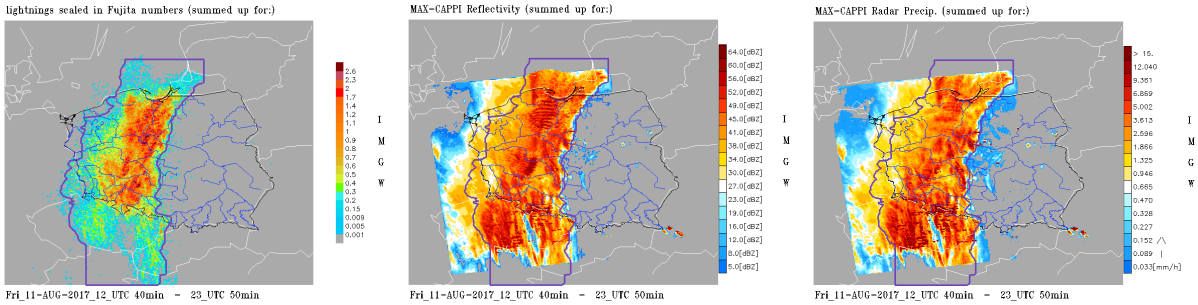

Fig. 3. The same as in Fig. 1, but for the time interval from 12:40 to 23:50 UTC on 11 August 2017, representing the third development stage of the considered MCS with the relevant three signature maps showing the severe thunderstorm activity connected with violent derecho episode.

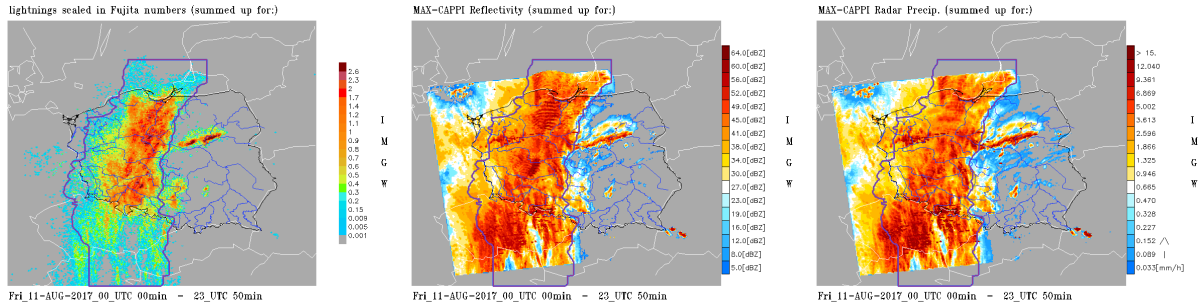

Fig. 4. The same as in Fig. 1, but for the time interval from 00:00 to 23:50 UTC on 11 August 2017 and three collective signature maps summarized this whole day.

(2021) and Wrona et al. (2022), that the first stage was "important for the development of the synoptic situation", which was also confirmed by weather reports from 10 August 2017 09 UTC to 11 August 2017 03 UTC given by the European Severe Weather Database and noted also by Lelątko (2020). In turn, the beginning of the third stage at 12:40 UTC was chosen because then the linear thunderstorm zone from South Bohemia changed the direction of its movement from the SEE-NNW to SSW-NNE. Later, this propagation direction remained unchanged until the end of the considered MCS episode, i.e., until 23:50 UTC.

To better explain the idea of determination of the used area mask to report the propagation path of the main MCS part/core during the whole day of 11 August 2017, the set of three collective signature maps is given in Fig. 4.

4. THE RESULTING MCS PROPAGATION PATH REFINED FOR THE DERECHO EPISODE

In principle, the MCS propagation path can be estimated from the wind trajectory, thunderstorm destruction path, and direct tracking of the movement of thunderstorm cells. Here, the latter idea was applied for the subjectively defined area of the main MCS electrical activity, limiting its range by a horizontal rectangle. The sides of such chosen rectangle coincide with the numerical grid of the operational COSMO model with the grid size of 2.8 km and are presented in Fig. 5. This rectangle is called farther the filter and is defined every 10 minutes according to

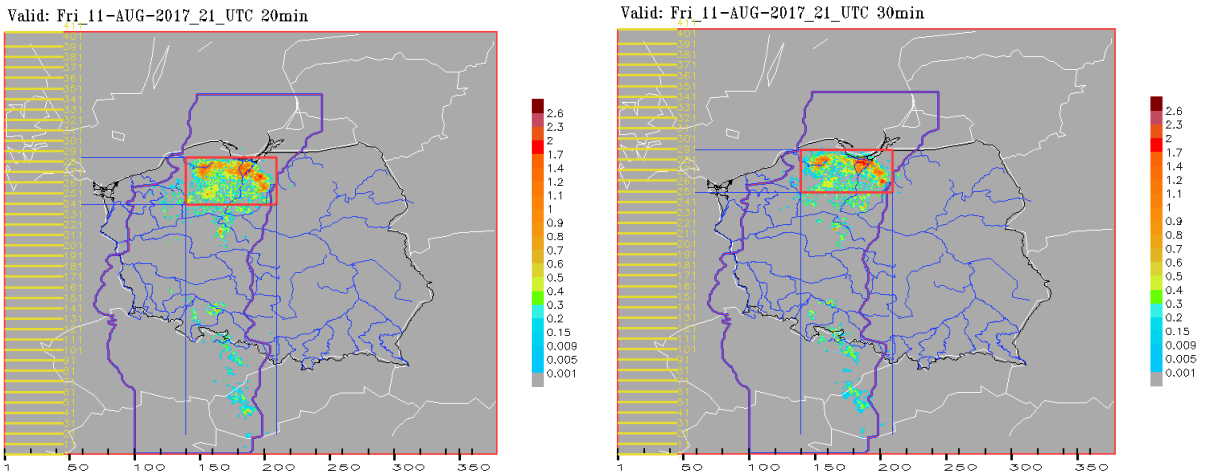

Fig. 5. The scheme presenting the idea of a movable filter as a useful tool that allows to evaluate the current location of the most active disturbance/convective area in relation to the used calculation grid. Here, the COSMO grid 2.8 × 2.8 km was applied. This example concerns two neighboring scans obtained at 21:20 and 21:30 UTC, that are given from left to right, respectively.

the PERUN lightning detection data converted to the relevant VFS numbers. The goal of this approach is to filter out all dispersed lightning discharges located outside the area of their main activity cluster and in order to focus on the impact of these not rejected flashes.

In Fig. 5, the *y*-axis of the used COSMO grid is parallel to the geographic north-south direction on the meridian of 10 degrees toward the east. Over Poland, the deviation of this axis from this direction does not exceed 10 degrees. Thus, it is sufficient to use the COSMO grid to describe the geographical orientation of the considered MCS propagation path. Moreover, the *y* coordinates given by the COSMO gird at the sides of the rectangle filter, i.e., (y_{min}, y_{max}), define the instantaneous range of the MCS displacement in this direction. Hence, as the MCS moves northward, these distinguished *y* coordinates are used to evaluate and monitor the speed of such propagation and to determine the overall impact range of the derecho dislocation/shift.

On the other hand, we define a few useful geometric objects to characterize the extent and structure of the considered MCS. The basic object is a rectangular filter, defined above and covering the entire compact/coherent part of the convection system. This method, denoted the main convective area domain, is assumed to be the geometric "gravity" center derived from the 10-minute VFS number distribution in the area delimited by the used filter. The next considered objects are two parts of this filter, i.e., its west and east sides/flanks. These flanks are the result of dividing the primary filter along the meridian of the COSMO grid passing through the center of "gravity" of the convection system. They also allow that the geometric location of the western and eastern flanks can be determined as the "gravity" centers related to the VFS numbers relevant to such parts of the considered convection system that are co-located, respectively, at its western and eastern side by the used filter. The locations defined in this way, enable us to evaluate the main trajectory of the convection system together with the trajectories of its flanks and to monitor the latitudinal extent of the whole moving system.

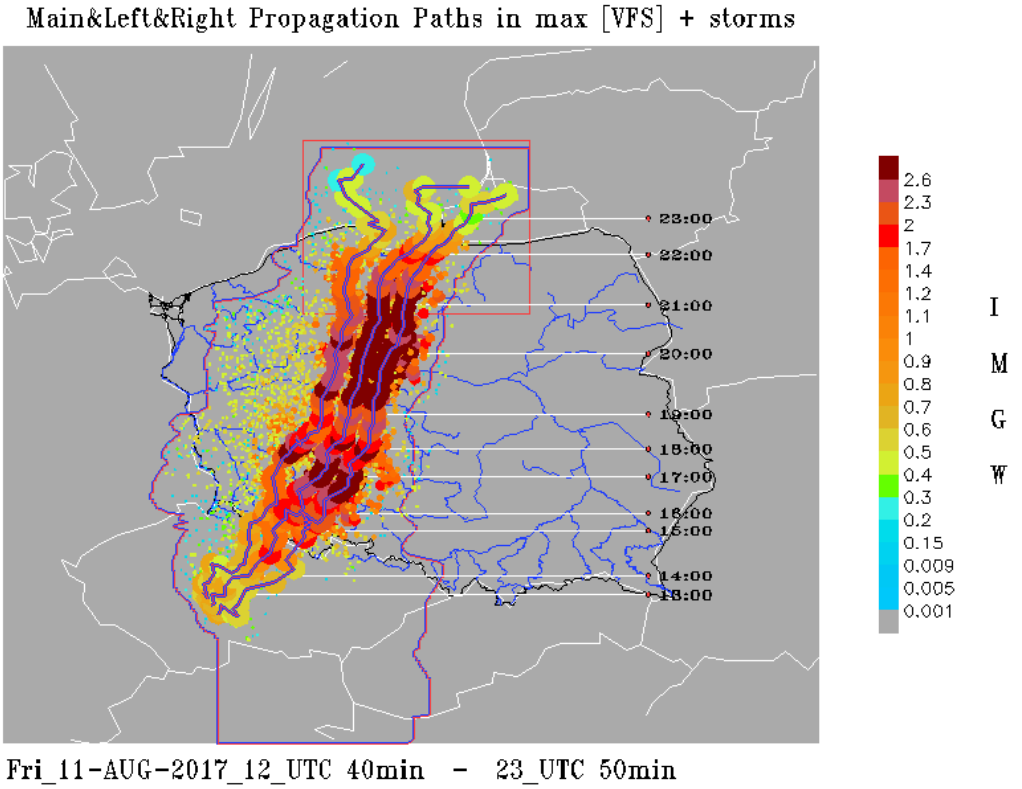

Fig. 6. Evaluation of the left, main, and right propagation paths of the whole considered MCS according to results obtained from the applied movable filter. More detailed description in the text.

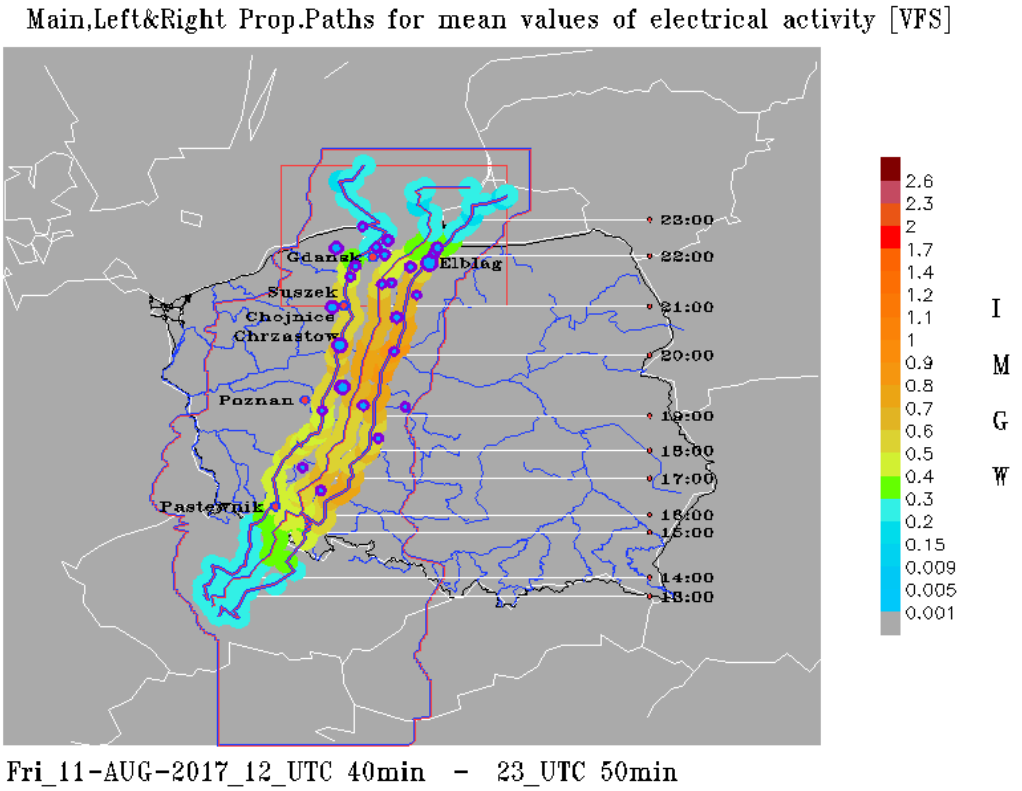

Fig. 7. The same as in Fig. 6, but for the result/change obtained from using the average VFS numbers for performing a movable filter. Blue dots indicated locations where gusts of wind were noted higher than 20 m/s. More detailed description in the text. Small pink dots stand for the Doppler radar locations.

Finally, we have shown in Figs. 6–7 the propagation paths of the whole considered MCS together with its left and right flanks. Figure 6 shows the trajectories superposed on 10-minute maximum VFS numbers for the entire system and its both flanks, respectively. But, in Fig. 7, such trajectories are superposed on the weighted average electrical/lightning activity along the whole system paths.

Figures 8–9 present the evolution of the maximum and spatially averaged VFS, i.e., the maximum of electrical activity for three types of the evaluated propagation paths of the considered convection system: main, western, and eastern. After 15:30 UTC, the time course of such electrical activity for all three types is similar, but around 17:00 UTC and after 20:00 UTC the noted dispersion is most meaningful. The first occurrence of local dispersion maximum at 17:00 UTC can be related to a supercell formation reported by Mańczak et al. (2021) and Wrona et al. (2022), while the second one, after 20:00 UTC and later, is caused probably by a significant detachment of a new thunderstorm cell evolving from the previous main propagation track of the considered convection system.

On the other hand, we can see in Fig. 10 that the eastern propagation path of the considered convection system is practically consistent with its main path throughout the entire analyzed time period and their courses are parallel, indicating similar VFS number changes, whereas the west track is consistent with the main track and together with the eastern track at most until 20:00 UTC. Such a time period ends with the wind gust record of 36.0 m/s in Chrząstów at 20:00 UTC. Let us add that this wind gust value is second in order, after the measurement of 42.2 m/s in Elbląg-Milejewo at 21:40 UTC. However, this maximum recorded wind gust that was noted later on, was related to the right propagation path of the considered convection system.

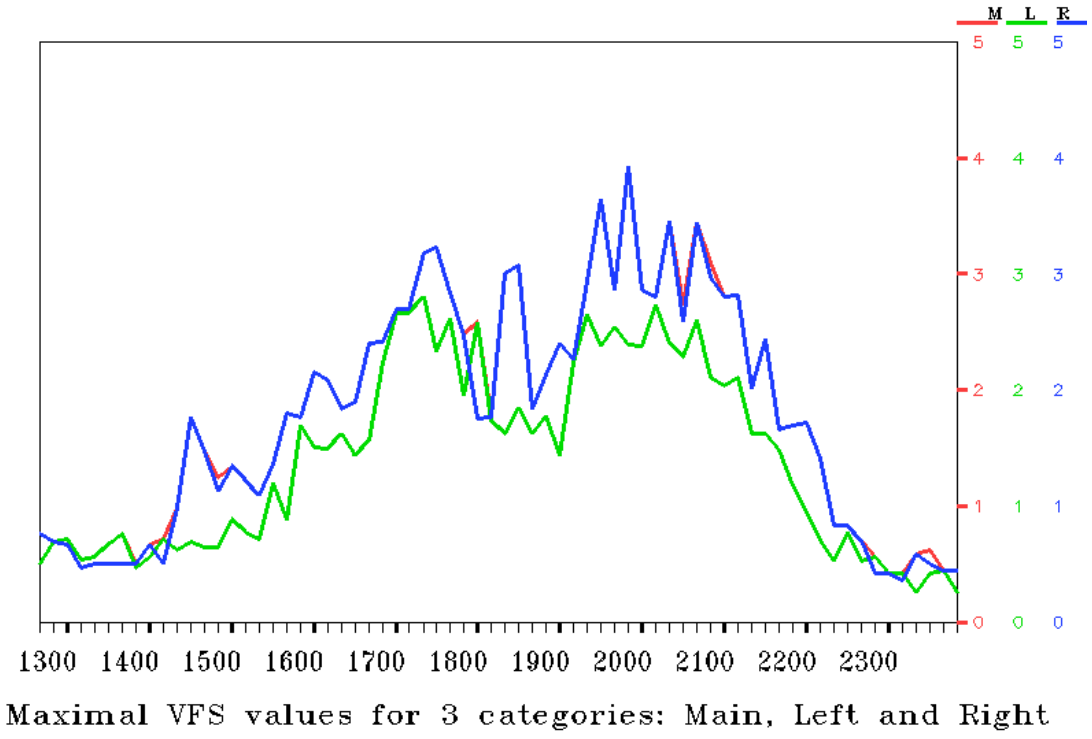

Fig. 8. The time evolution of the maximum VFS number evaluated in the successive windows/slots of the used moveable filter during the propagation paths of the considered convection system: Main (red), Left/west (green), and Right/east (blue). Note that the maximum VFS number for the Main and Right paths practically coincide.

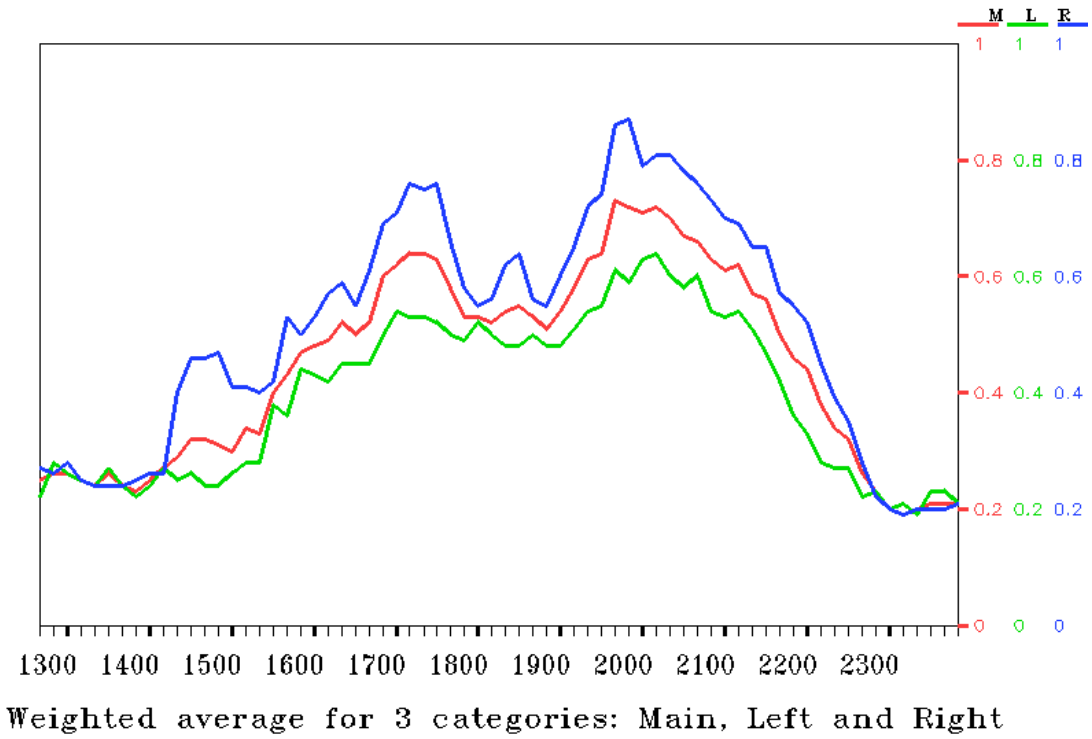

Fig. 9. The same as in Fig. 8, but concerns the time evolution of the spatially averaged VFS number for three types: main, left, and right propagation path of the considered convection system, denoted by red, green, and blue curves, respectively.

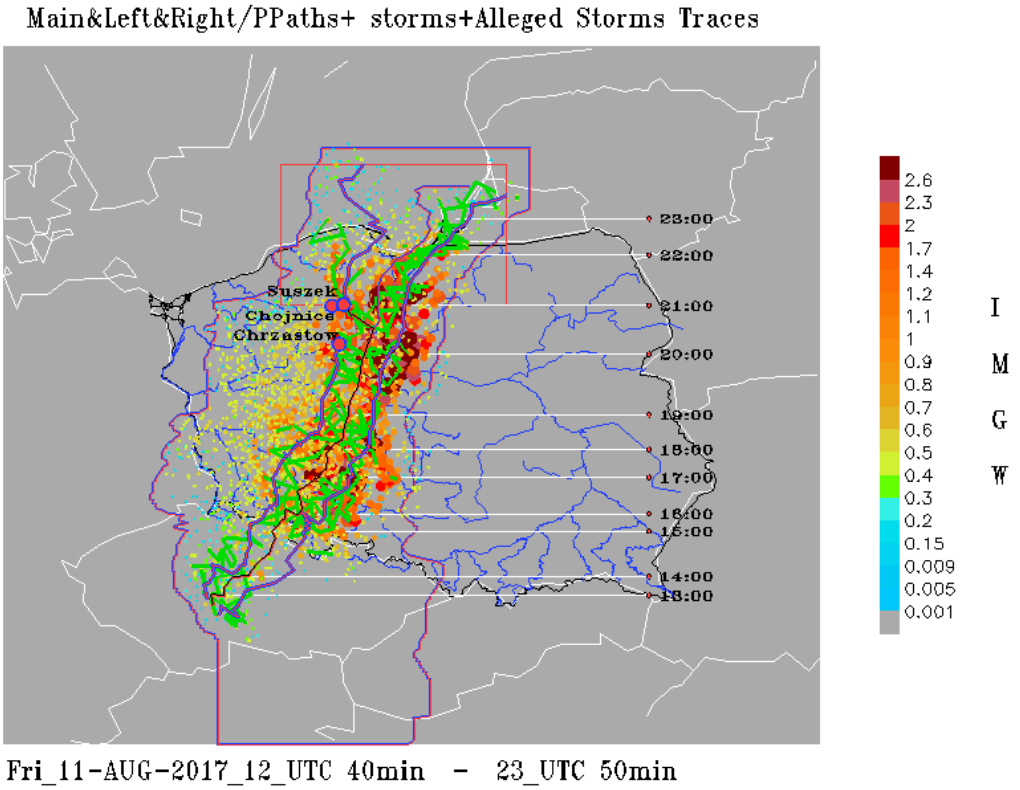

Fig. 10. The same as in Fig. 6, but shows the background of three propagation tracks of the considered convection system marked by blue-purple lines. This background consists of the reduced lightning hot points given by color and size according to the VFS number scale, while visible green lines link the locations with the extremely high VFS number, i.e., lightning hot points noted at the adjacent time terms. Three sites Chrząstów, Chojnice, and Suszek, where the devastating wind gusts have been noted, are indicated by pink circles.

It should be noted that the electrical activity of the western flank of the considered convection system, noted in the time period from 20:00 to 21:00 UTC, deserves a more detailed analysis (see the set of five maps presented in Fig. 11). Focusing on the western part of the system, i.e., the vicinity of Chrząstów, Chojnice, Suszek, and Rytel, we can notice that the electrical activity noted at these sites fluctuates distinctly. At first, it is intense at the exit from Chrząstów, then weakens, reaching the minimum at 20:40 UTC, and 20 minutes later it gains strength in the vicinity of Chojnice, Suszek, and Rytel. Further away, it detaches from the mainstream and advances north, maintaining its strength and distinctiveness. Such analysis of electrical activity changes, given in Fig. 11, can suggest that the westernmost area of the electric activity detaches from the main core of the considered convection system before 21.00 UTC. On the other hand, the re-analysis of the situation given in Figs. 6–7, which has indicated the sharp western bent of the left flank trajectory at 20:40 UTC, suggests that it can be considered as the occurrence of a propagation path splitting for the whole convective system.

We assume that a probable cause of the occurrence of such MCS split at 20:40 UTC is resulted from the additional presence of a mesocyclone system in the considered area and given in Figs. 11–13. Such mesocyclone was also recognized on radar scans by Taszarek et al. (2019a,b) and then analyzed in detail by Łuszczewski and Tuszyńska (2021). In turn, the considered split process was limited territorially by the site locations of Rytel, Suszek, Chrząstów, and Bydgoszcz. However, the range of the Poznań and Gdańsk radars rather does not allow for a detailed reliable analysis of the mesocyclone development in this area. Hence,

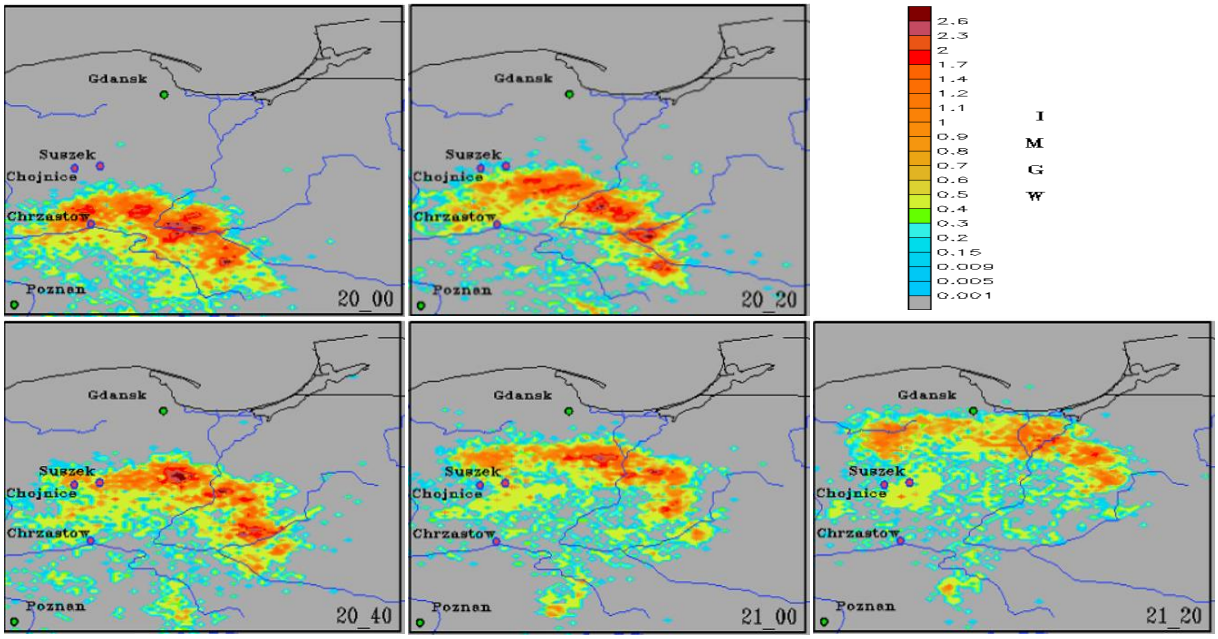

Fig. 11. Set of five maps presenting the evolution of VFS number changes in the vicinity of Chrząstów, Chojnice, and Suszek from 20:00 to 21:20 UTC with the 20-minute time step. The scale of noted VFS number is given by the colored bar. These maps are a necessary supplement to Figs. 6–10 in order to determine precisely the time moment of splitting propagation paths of the considered convective system. More detailed scenario of such split trajectories is depicted in Fig. 12.

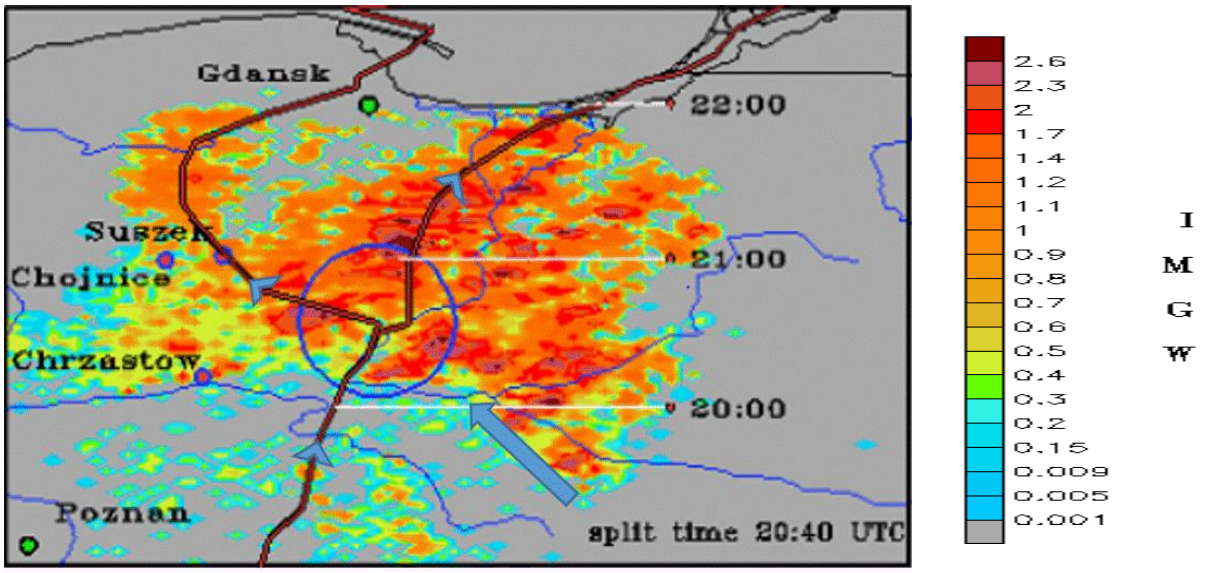

Fig. 12. The scenario of split trajectories of the considered convective system at 20:40 UTC, as the resumption result of five maps given in Fig. 11.

an attempt was made to identify thunderstorm cells at the adjacent dates and recreate their trajectories based on the PERUN lightning detection data that confirmed initially the split occurrence. But such an approach was not straightforward. Thus, forced by the necessity to depart from the pure phenomenology, simulations obtained from the relevant COSMO_2.8 km model were analyzed. These simulations, which routinely started from 18:00 UTC and produced "forecast" fields for the next 6 hours, reproduced unexpectedly well the mesocyclone development

process and confirmed the earlier locations of this mesocyclone system given by the relevant Doppler radar products. We presented in Fig. 13 the enlarged (zoomed) space domain together with the considered split occurrence at 20:45 UTC. There we can see the projection of the maximum values of the vertical component of vorticity on the XY and ZY planes, while the barbs illustrate the appropriate wind field at the altitude of 10 km. Here, yellow barbs denote "true wind" in the absolute motion and black ones denote wind in the relative motion to the whole system motion, defined as the absolute motion and reduced by its averaging. These latter well emphasize the properties of the shear-related vorticity. It should be noted that the absolute-motion of the considered air mass turned westward just behind the area of increased vorticity that matches the independently determined propagation path of the western part of the considered convective system to its strong electric activity. Moreover, the relative-motion of air mass agrees well with the whole vorticity pattern. On the other hand, the discussion with experts on the subject pointed to the possibility that the potential MCS split observed by the relevant electric activity changes related to their used pattern may have different characteristics and concern different and higher thundercloud areas in comparison to the occurrence MCS split observed by radar and concerning such cloud regions with a large density of the big-size cloud particles. Hence, the wind field at height of 10 km presented in Fig. 13 corresponds well to the inferred MCS propagation path and changes evaluated from the noted electric activity during the MCS development.

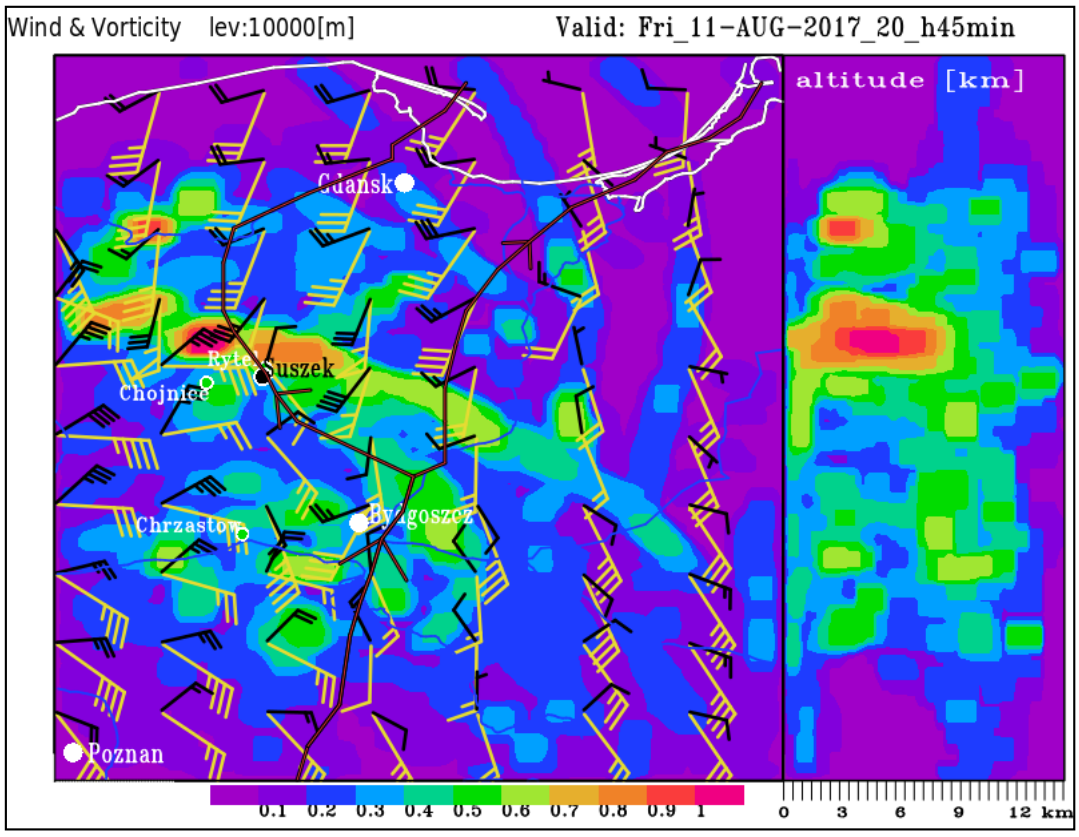

Fig. 13. Projection of the maximum values of 3D vorticity, i.e., the vertical component of the rotation of wind velocity vector multiplied by the scale factor of 2.6×10^3, on the XY and ZY planes. The color and numerical scale of the considered air vorticity is given at the bottom of the XY plane. Additionally, on the XY plane, the wind marked by yellow barbs indicates the absolute air motion/flow and the wind marked by black barbs indicates the relative air motion/flow given for 11 August 2017 at 20:45 UTC for a height of 10 km. Other topographic details superimposed on the XY plane are the same as in Fig. 12.

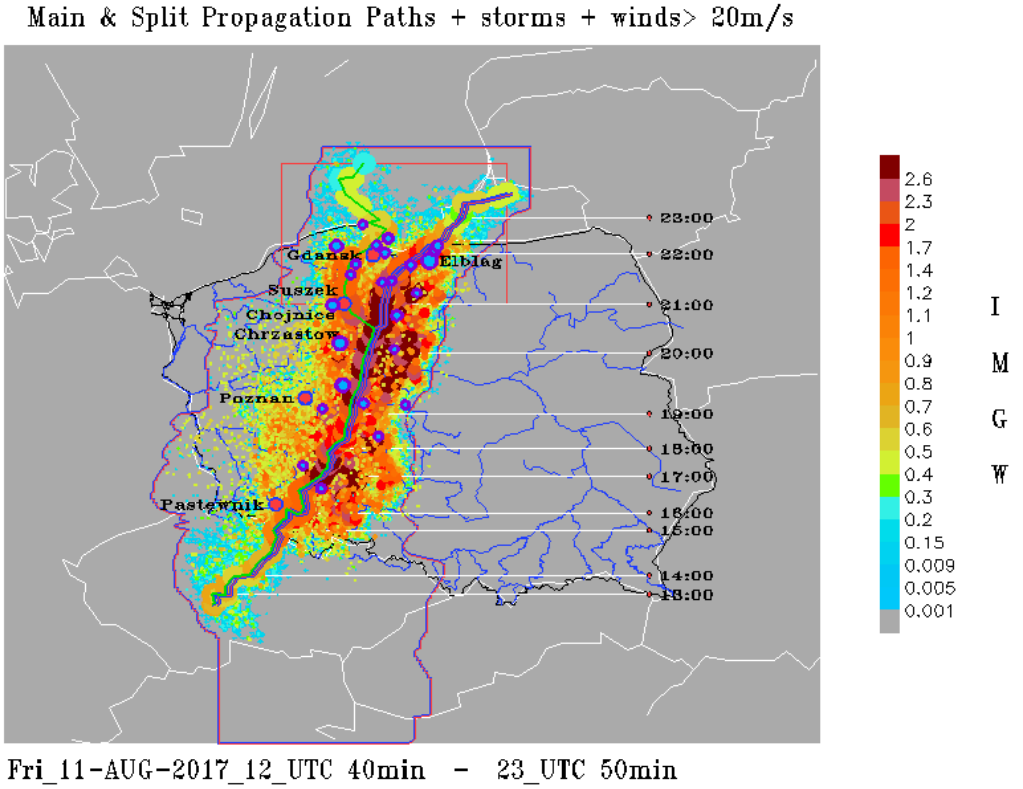

Fig. 14. Main and left propagation paths of the considered MCS with final derecho episode. These paths are overlapped on the MCS electrical activity given in the relevant VFS number indicated by colored bar. Here the wind gusts greater than 20 m/s are marked by blue and violet circles, whose sizes are proportional to the wind strength. Four pink circles show the Doppler radar locations.

The summary result of the analysis performed by us and presented previously in Figs. 6–13 is given in Fig. 14. Here, three hypothetical propagation paths of the considered MCS, in the sense of their physical distinctiveness, were reduced to a single lane with the denoted one split. However, the main path of the MCS has been preserved and additionally marked, because it practically coincided with the MCS eastern propagation path. It is shown as the bold purple line superimposed on the set of separated blue circles, that converged into the single serpentine line and is colored according to the maximum VHS number evaluated for each of the used 68 primary scans. Whereas the thin green line corresponded to the western flank of MCS in accordance with the previous analysis and should coincide with the main MCS track, at least until 20:00 UTC. This can mean that at this time the MCS moving over Poland was compact and without any split. But in the time span from 20:00 to 21:00 UTC, or possibly earlier, if we take, in accordance to Łuszczewski and Tuszyńska (2021), that 19:10 UTC has been the beginning of the MCS split indicated by radar data, it can be seen from Figs. 11 and 12 that the formation of a new separate thunderstorm area was focused at Suszek. Such a thunderstorm area kept its subjectivity (coherence) during its farther northward movement. Hence, the Suszek site can be considered as the location where a detachment or split process of the primary formation of MCS occurred. It is worth relating this MCS split place to possible interaction with the mesocyclone formation given in Fig. 13. Summarizing, the green line that detached from the main MCS path and is shown in Fig. 14 can be understood as a side path of the derecho disturbance. In Fig. 14 there are also indicated 24 different sites where the telemetric measurements of wind gusts exceeding 20 m/s were reported by Mańczak et al. (2021) and Wrona et al. (2022). Although these characteristic wind gust records were noted on both sides

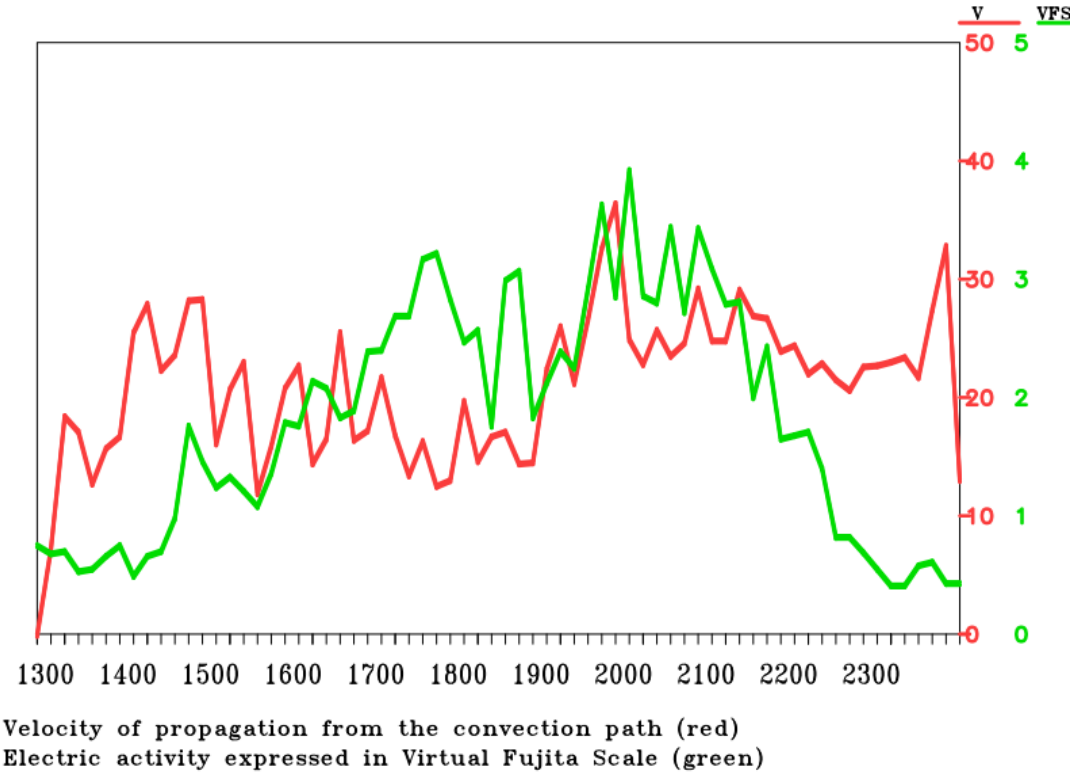

Fig. 15. Synchronous graphs/courses of the MCS propagation velocity and the MCS electrical activity for the considered MCS case on 11 August 2017 in the time interval from 12:40 to 23:50 UTC.

of the main MCS track, the wind activity on its west side correlated more clearly with the most spectacular casualties and damage caused by the considered derecho episode, e.g., in the Tuchola Forest. In turn, the derecho electrical activity prevailed certainly on its eastern flank. For understandable reasons, most of the attention in the papers cited above was focused on the analysis of the western flank, which was also better, but not fully and satisfactorily, documented by radar data from Poznań and Gdańsk.

The eastern and right side of the MCS propagation path presented in Fig. 14 was expressed in the coordinates of the COSMO_2.8 km model and then was used to determine the propagation speed of the whole convection system. This propagation speed calculation was based on the particular locations of such a system, changing in ±10 minutes relative to the given/chosen time moment. The final plot of the variation of MCS propagation velocities obtained for its main path together with changes of the maximum VFS number indicated the MCS electrical activity in the considered MCS area and in the time interval from 12:40 to 23:50 UTC are presented in Fig. 15. The highest estimated MCS propagation speed, up to 40 m/s, occurred around 19:30 UTC and preceded the MCS path split. Additionally, three general characteristics of the MCS with derecho episode, namely, the travelled distance, the time duration, and the average propagation speed, were estimated at 864.42 km, 11.17 hours, and 77.4 km/h, respectively.

5. EVOLUTION OF THE MCS WITH DERECHO EPISODE REFINED FROM ITS LIGHTNING DISCHARGES ACTIVITY AND RELATED TO THE PERFORMED COMPUTER SIMULATIONS CONTEXT

The performed computer simulations of the derecho day at 12:00 and 18:00 GMT enable us to interpret the detected lightning activity of the MCS in a broader synoptic context. Here, the starting point is the proven diagnostic tool, i.e., the operational forecast of turbulence potential,

used by the Polish internet pages awiacja_imgw_pl since 2012 and given by Parfiniewicz and Bojanek (2013). The turbulence potential (*PT*) is expressed as a weighted average of two rudimental numbers relating to turbulence, i.e., the Reynolds number (PT_{Re}) and the Richardson number (PT_{Ri}). The formula in Fortran notation for the *PT* parameter can be roughly written as:

$$PT(i,j,k) = \mathrm{SQRT}([PT_{\mathrm{Re}}]**2 + [PT_{\mathrm{Ri}}]**2)/\mathrm{SQRT}(2.) \ ,$$

where

$$[PT_{\mathrm{Re}}] = (Ro(k)*V(i,j,k)/\mathrm{skala});\ \mathrm{skala} = 1.\ [\mathrm{kg/m^3}]*30.\ [\mathrm{m/s}]$$

$$[PT_{\mathrm{Ri}}] = (Ro(k)*dV/dz(i,j,k)/a_{\min}1(1.,(0.5 + a_{\max}1(0.,\mathrm{amin1}(1.,3.33*\mathrm{Ri(i,j,k)}))))) \ / \ \mathrm{skala}$$

$$[RoV] = (Ro(k)*V(i,j,k)/\mathrm{skala});\ \mathrm{skala} = 1.\ [\mathrm{kg/m^3}]*1.\ [\mathrm{m/s}]$$

In turn, the additional parameter PT_{Re} per *RoV* can be taken as a calibrated air flow momentum for the considered convective system, where *Ro* stands for the air density and *V* is the 3D air velocity, whereas the PT_{Ri} represents a balanced convection scale, i.e., the air buoyancy versus air flow shear normalized by the scaling factor (skala). However, important in terms of the synoptic approach are, as always, the pressure parameter (*p*3*D*), especially this brought to the sea level [Pmsl], and the distribution of potential temperature parameter (teta), directly related to the height of the tropopause. Since the subject of the considered synoptic process turned out to be a supercell that was created around 17:00 UTC and retained its subjectivity at least until 24:00 UTC during the derecho episode, its rotation (left or right-handed) might be identified as the horizontal vorticity at the mesh model nodes, denoted by *Rot*. The intensity of the considered convection process may be also directly diagnosed by the vertical flow rate parameter *W*.

5.1 The first-stage development, from 12:40 to 15:50 UTC, and the early stage of a supercell formation

We have chosen 12:40 UTC as the beginning of the considered derecho incident. Then the linear thunderstorm zone from South Bohemia changed the direction of movement from SEE-NNW to SSW-NNE. In practice, this propagation direction remained unchanged until the end of the derecho episode, i.e., until 23:50 UTC. The propagation path of the MCS as a whole was presented with details in Section 4. Until 14:00 UTC the linear thunderstorms zone, arranged perpendicular to the propagation, was on the Czech side, approaching the Sudetes (a mountain range constituting the Polish-Czech border). The process of overcoming the mountain barrier ended at 15:50 UTC. At that time, the whole of Lower Silesia region was in a stormy area, with two characteristic and separate lightning patterns grouped in the vicinity of the Kłodzko Valley (see the map at 15:50 UTC in Fig. 16) and far west of the Moravian Gate, that was usually privileged when convection flew from the Czech side. To conclude the consideration of this stage, it is worth noting that the maximum peak values of lightning discharge activity, given in Fig. 16 by changes of the relevant VFS number, increased from 0.5 at 13:50 UTC in the area of Prague, in the Czech Republic, to 1.8 at 15:40 UTC in the Kłodzko region, in Poland. The whole course of this early, convective stage development is presented in Fig. 16 by the set of four selected maps showing changes of the equivalent VFS number obtained during the 10-minute time interval.

The related synoptic context of the considered MCS convection process in the time interval from 12:40 to 15:50 UTC is summarized by the relevant set of four maps for *p*3D, (teta), *W*, and *RoV* parameters simulated at 15:45 UTC and shown in Figs. 17–20, respectively.

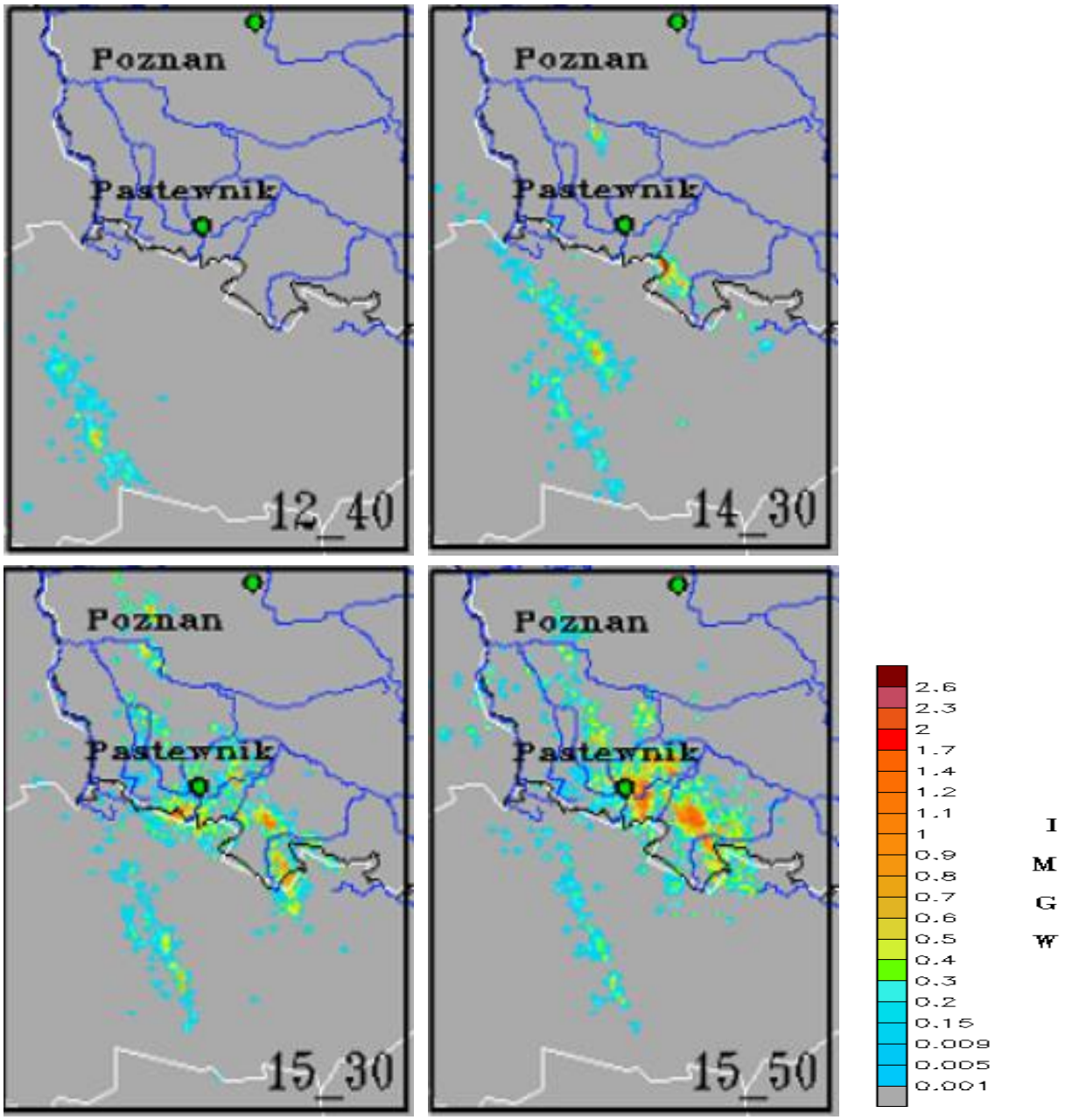

Fig. 16. Set of four selected maps indicating changes of the equivalent VFS number obtained during the 10-minute time interval and evaluated at 12:40, 14:30, 15:30, 15:50 UTC, respectively, and illustrating the first stage of MCS development.

Basing on the relevant air flow field patterns given in Figs. 17–20 we can note that a characteristic feature of the considered MCS convection process during its early development stage with a supercell formation was firstly connected to the deepening of the pressure depression and formation of ground-level convergence zones, as shown in Fig. 17; secondly – to a lowering of the tropopause height on the derecho track and covering the areas of Wrocław and Poznań from the west side, as presented in Fig. 18; thirdly – to an increase of the vertical air velocities in the area of Wrocław and Poznań, as given in Fig. 19; and forthly – to an increase of the air flow momentum strength from the west together with the formation of a "wind hammer" in the Wrocław-Poznań region, as depicted in Fig. 20.

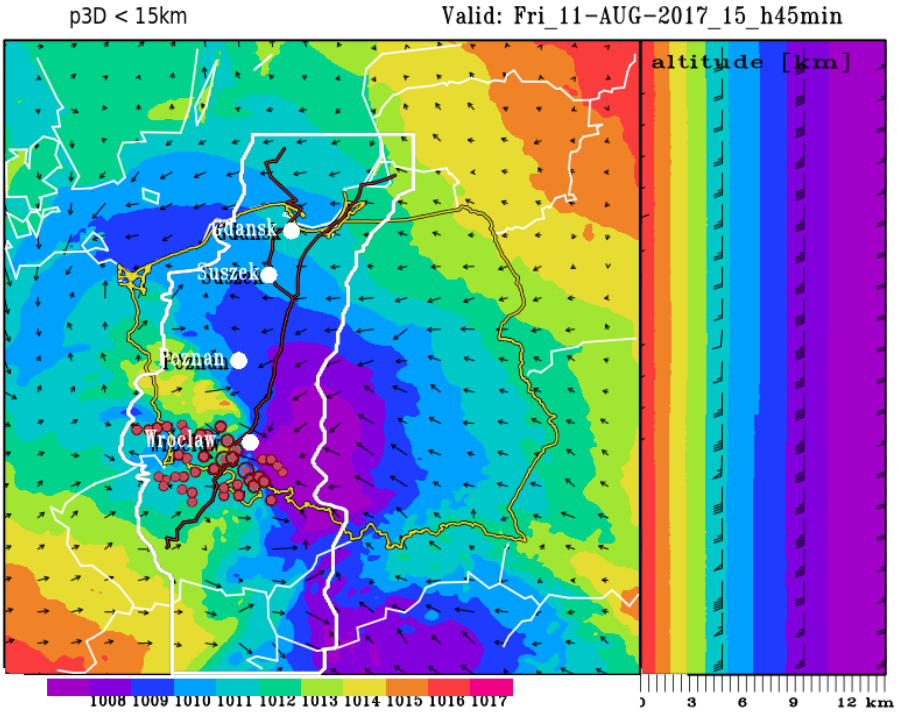

Fig. 17. The simulated map of the *p*3*D* parameter calculated for 15:45 UTC and shown in the XY and ZY planes. The color and numerical scale in hPa units is indicated at the bottom of the XY plane. The relevant wind pattern (in knots), for its horizontal components (*u*, *v*), is indicated by black vectors in the XY plane and by barbs for its vertical components (*w*, *v*) in the ZY plane. Additional topographic details superimposed on the XY plane related to the considered MCS path with spilt incident are the same as in Fig. 14. In turn, the set of small and bigger red dots presents the locations of lightning activity sources detected at 15:45 UTC, whose size is in the accordance to the calculated VFS numbers in the particular location area.

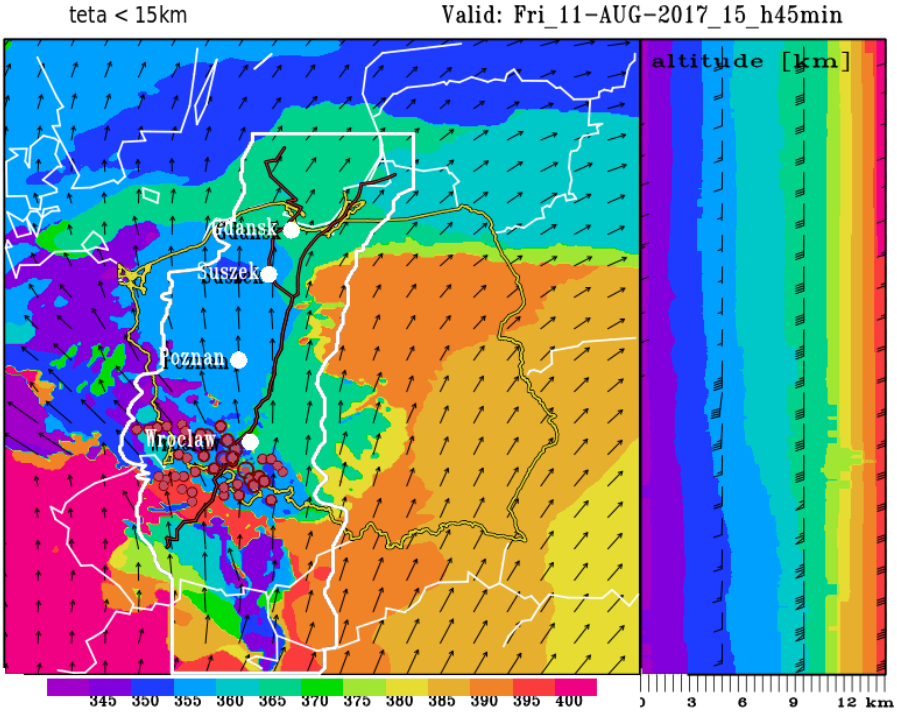

Fig. 18. The same as in Fig. 17, except of the pattern for the simulated map of the (teta) parameter calculated at 15:45 UTC, and the color and numerical scale indicated in °K unit.

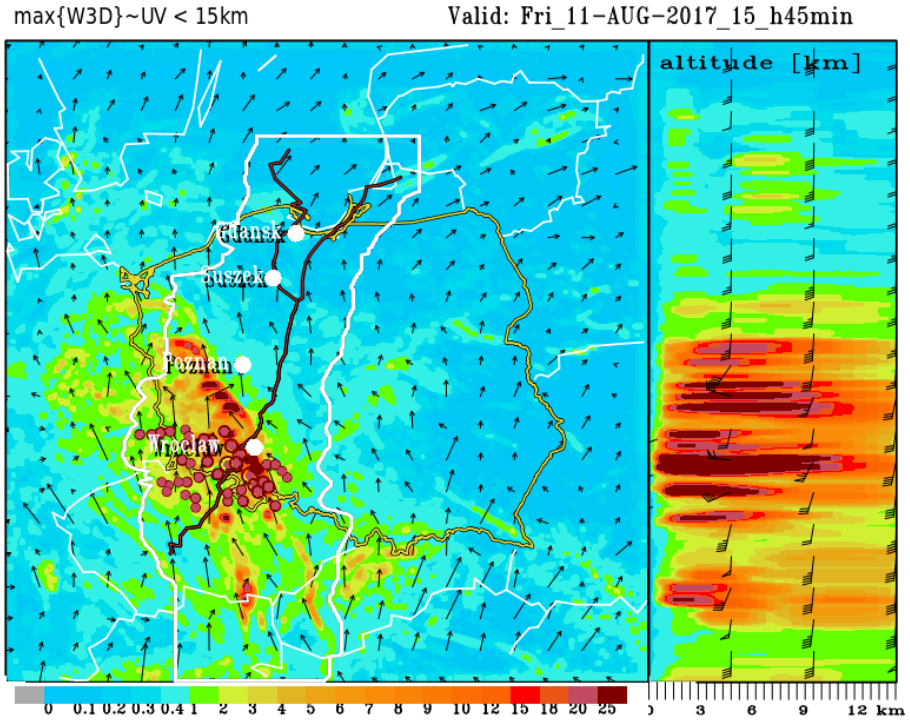

Fig. 19. The same as in Fig. 17, except of the pattern for the simulated map of the *W* parameter calculated at 15:45 UTC, and the color and numerical scale indicated in knots.

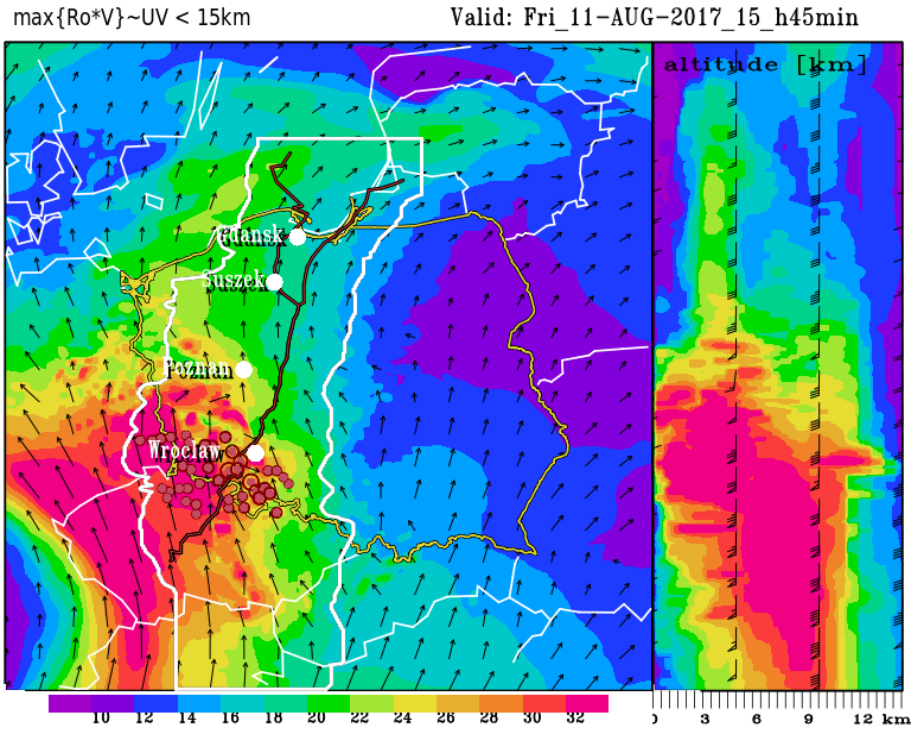

Fig. 20. The same as in Fig. 17, except of the pattern for the simulated map of the *RoV* parameter calculated at 15:45 UTC, and the color and numerical scale indicated in formally dimensionless units (due to the normalization of *RoV* by a scaling factor (skala = 1. [kg/m^3]*1. [m/s]), which numerically reduces this expression to a calibrated by density air flow).

5.2 The second stage development, from 16:00 to 17:30 UTC, and further supercell consolidation

We can talk about an earlier evolution of a derecho incident over Poland from 15:50 UTC. The considered MCS route, just from this time moment, takes place over Poland territory. In turn, from 16:00 UTC we have observed a fluctuating increase in the electric activity reaching the relevant VFS number equal to 2.4 at 16:40 UTC. After that, the value of VFS number increased sharply to 3.23 at 17:30 UTC (see Fig. 22). Hence, we can presume that this electric activity stage of the MCS is connected to its consolidation process into a supercell form, as reported by Łuszczewski and Tuszyńska (2021). Indeed, as can be seen from the Poznań radar data, at this time the considered MCS makes its overshooting to the stratosphere, as shown in Fig. 21.

Here, it should be noted what happens during this MCS development stage over the Silesian Lowlands region, where the MCS consists of two separated convection cores indicated in Fig. 22 by the map at 17:30 UTC. They are located in the NW and SE sectors, respectively, while the one from the SE sector is electrically more active, with a set of two-chamber/twin storm cores indicated by the evaluated VFS number equal to 3.23 and having two convection shafts. It can be interesting to notice and probably it is a characteristic feature for such a development stage of the considered MCS formation that the building-up phase of its electrical activity is finished in a significant decrease of the MCS propagation speed. This might mean that the considered two storm cores could possibly slow down the expected jet stream support for a further development of the MCS. But unfortunately, it does not happen at that time. This was verified and confirmed by the course of the considered MCS development process that lasted from 16:00 to 17:30 UTC and is presented in Fig. 22 by the set of five maps indicating the particular change of the relevant VFS number evaluated in accordance to the PERUN lightning detection data given in the real time.

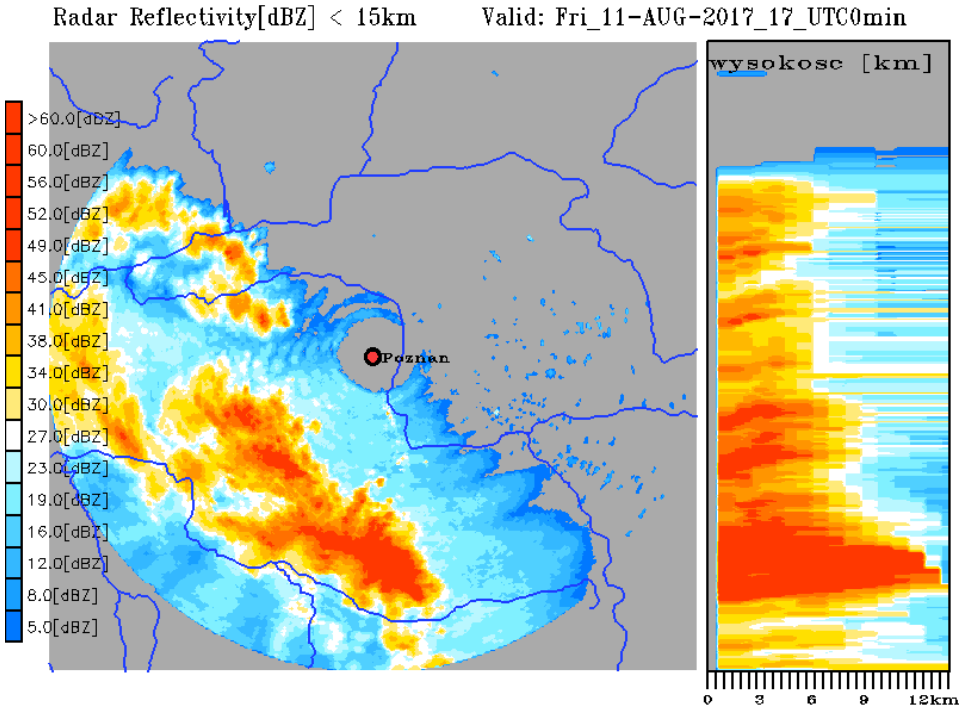

Fig. 21. Quasi 3D scans of radar reflectivity data obtained from the Poznań radar at 17:00 UTC. These radar scans were also preceded by the interpolation of the measured radar reflectivity in the altitude range from 1 to 18 km and the grid step of the XY plane of about 0.7 km, similar to the computational grid COSMO_2.8 km model with Δz = 250 m.

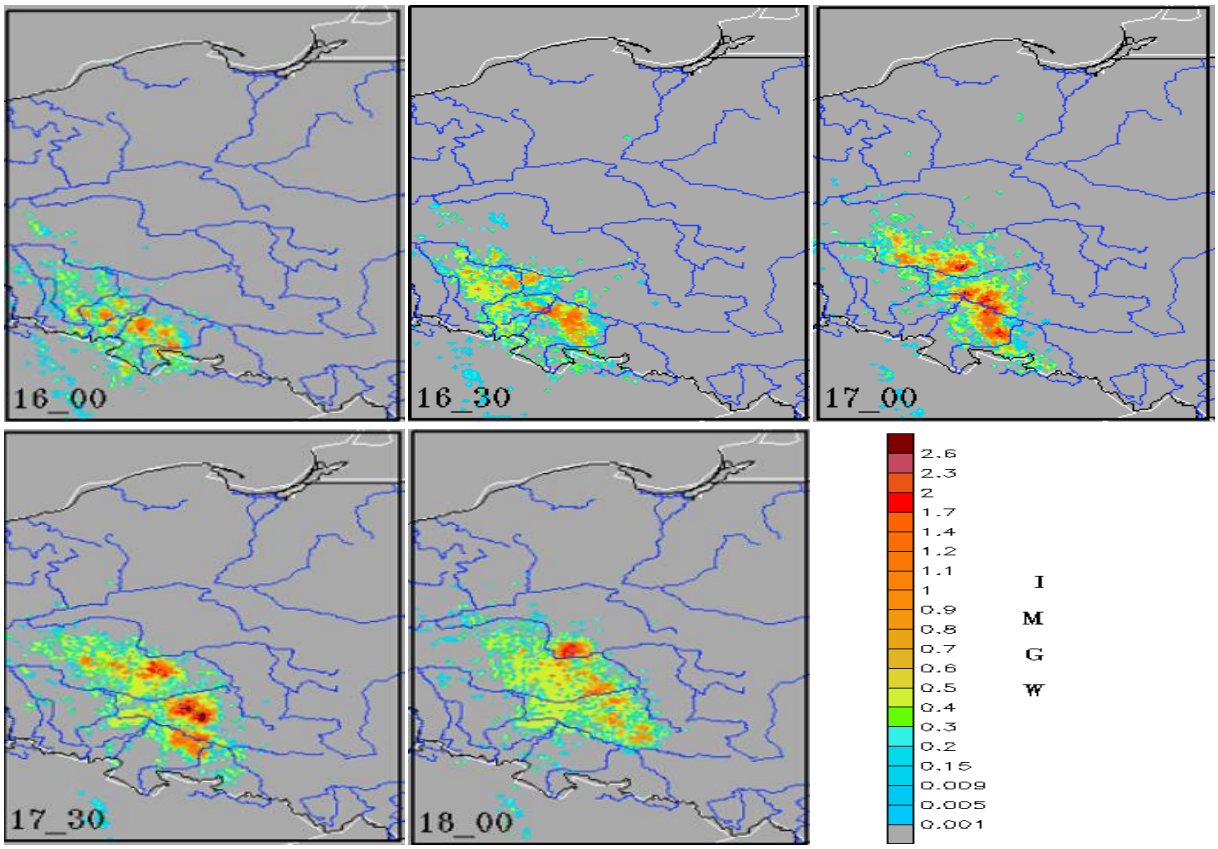

Fig. 22. Set of four selected maps indicating changes of the equivalent VFS number obtained during the 30-minute time interval and illustrating the second stage of MCS development lasting from 16:00 to 17:30 UTC. The additional fifth map just shows the transformation of MCS to its structure noted at 18:00 UTC and starting the next and later MCS development stage.

The relevant synoptic context of the following development of the considered MCS convection process in the time interval from 16:00 to 17:30 UTC is summarized by the next set of four maps for *p*3*D*, (teta), *RoV*, and *Rot* parameters simulated at 17:00 UTC and shown in Figs. 23–26, respectively. Additionally, the METEOSAT SEVIRI color-enhanced IR brightness temperature image showing the exact location of the supercell formation over Poland on 11 August 2017 taken from the EUMETSAT 2017 database at 17:00 UTC is given in Fig. 27.

Taking into account the air flow field patterns given in Figs. 23–26 we can note that a characteristic feature of the considered MCS convection process during this development stage involves further supercell consolidation. This consolidation was connected to: first – the deepening of the pressure depression with an extremely strong ground-level convergence zone, as shown in Fig. 23; second –the lowering of the tropopause height that coincided, in the XY projection, with such supercell formation covering the regions of Poznań and Wrocław, as presented in Fig. 24; third – to the formation of a stream air flow transferring energy from the upper atmosphere to the ground layers, as given in Fig. 25; and fourth – to the increase in negative rotation airflow, indicating that the positive left-handed flows which prevailed at the beginning were gradually followed by negative right-handed flows, as shown in Fig. 26.

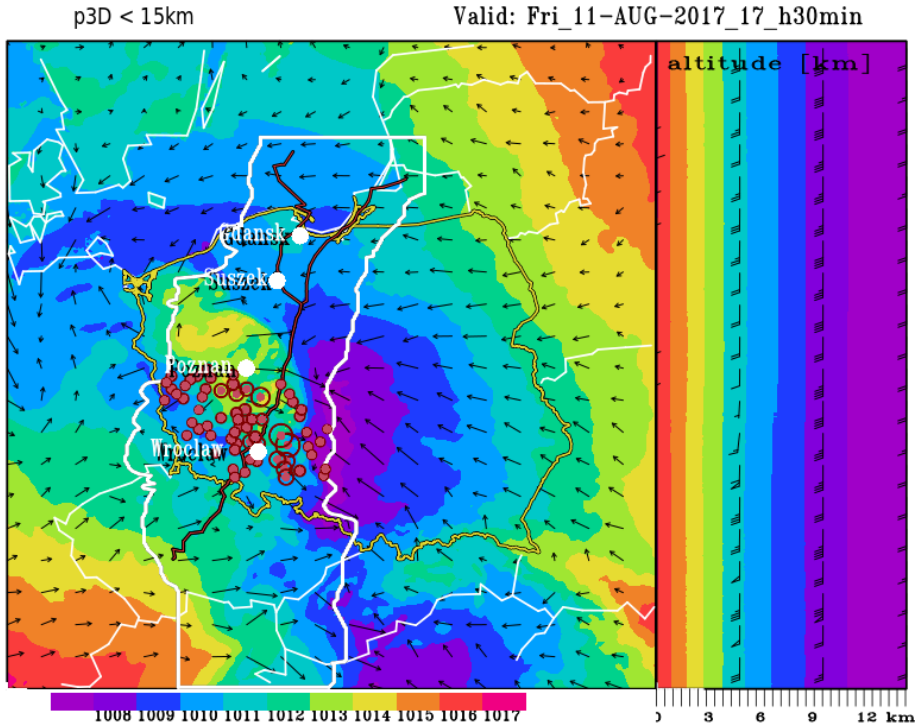

Fig. 23. The same as in Fig. 17, except for the pattern for the simulated map of the *p3D* parameter and lightning activity calculated at 17:30 UTC.

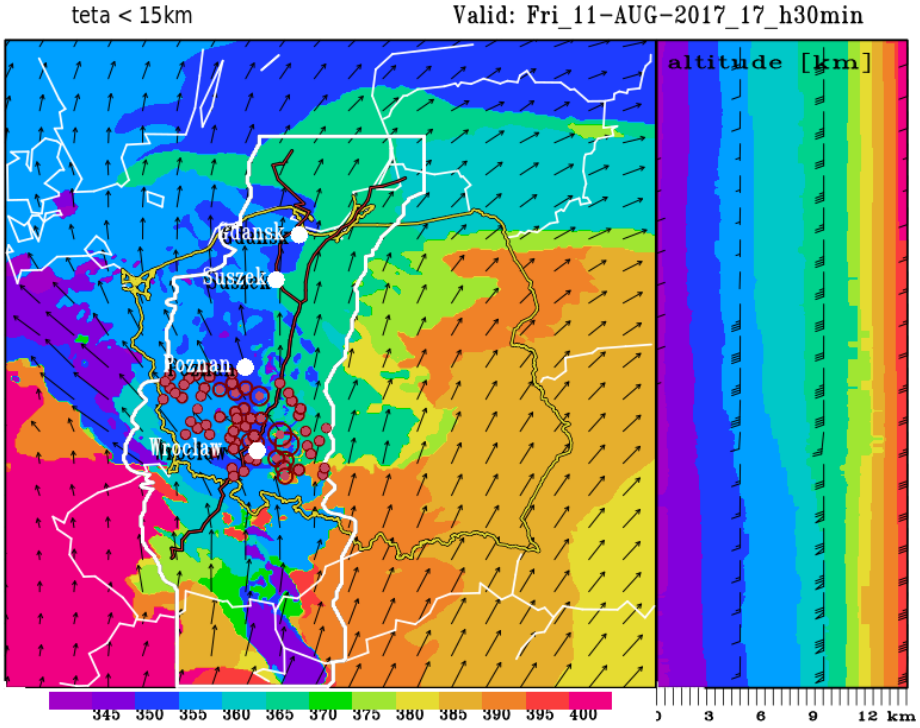

Fig. 24. The same as in Fig. 23, except for the pattern for the simulated map of the (teta) parameter and lightning activity calculated at 17:30 UTC.

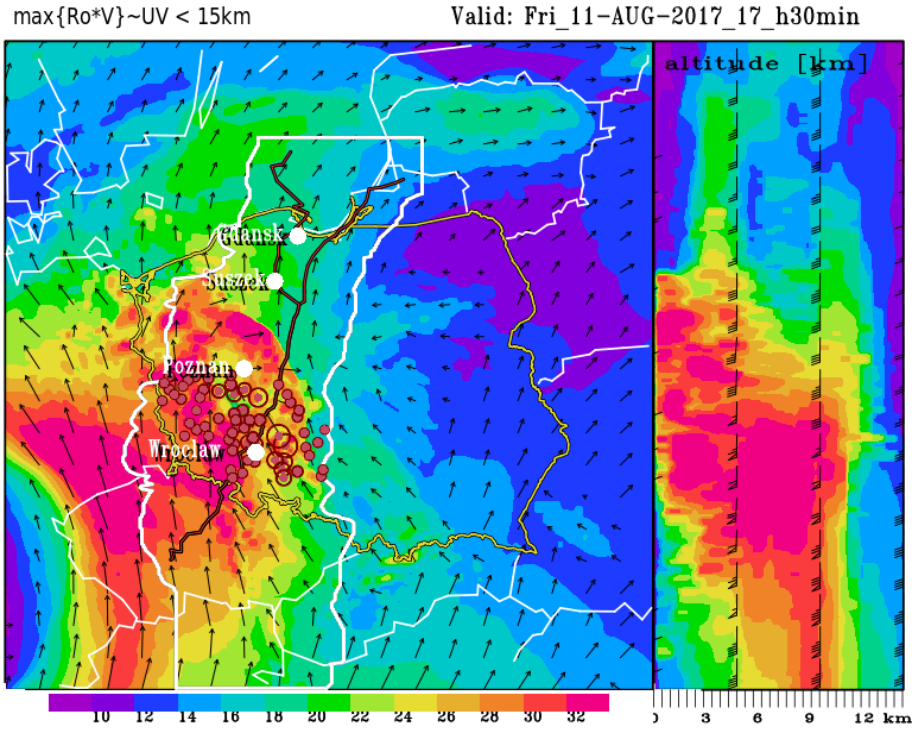

Fig. 25. The same as in Fig. 23, except for the pattern for the simulated map of the *RoV* parameter and lightning activity calculated at 17:30 UTC.

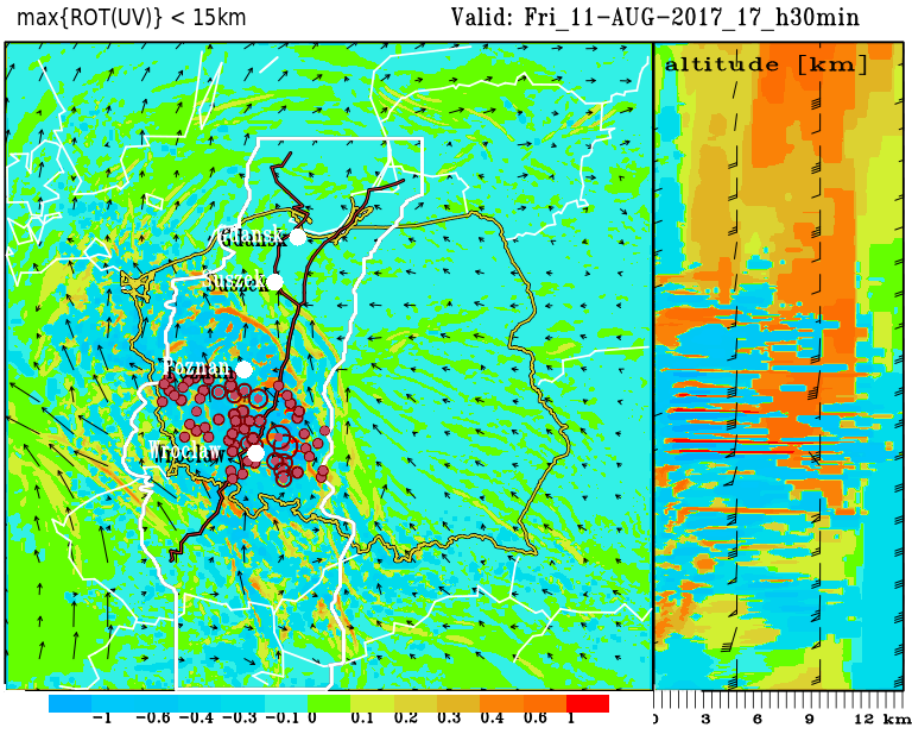

Fig. 26. The same as in Fig. 23, except for the pattern for the simulated map of the *Rot* parameter and lightning activity calculated at 17:30 UTC.

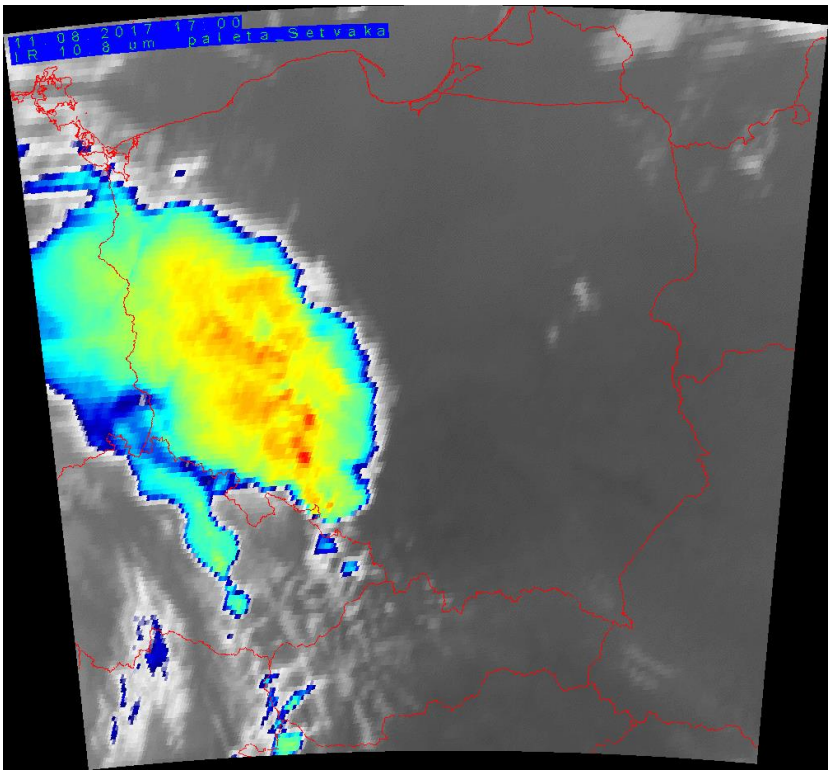

Fig. 27. METEOSAT SEVIRI color-enhanced IR brightness temperature image of the considered supercell formation over Poland on 11 August 2017 taken from the EUMETSAT 2017 at 17:00 UTC (© EUMETSAT 2017, © dane.sat4envi.imgw.pl, © OpenStreetMap contributors, reported also by Łapeta et al. (2021)).

5.3 The third stage development, from 17:30 to 21:00 UTC, together with the MCS split episode at 20:40 UTC

Let us define now the considered MCS as the set of convective nuclei (cores) of an evolving supercell. After 17:30 UTC, further MCS consolidation took place. In the considered time period, two separated strong convective areas of thunderstorm lightning activity have merged into one coherent and huge convection region, where the dominance of the NW located thunderstorm pattern was noted and presented in Fig. 22 by the map given at 18:00 UTC. Moreover, ten minutes later, at 18:10 UTC, we recorded the minimum VFS number equal to 1.77, that later on rapidly increased, reaching the local maximum of 3.08 at 18:30 UTC, which was shown in Fig. 15.

At 19:10 UTC dense/compact lightning discharge zones occurred east of Poznań and were stretched linearly from SE to NW (see Fig. 28). The further evolution process of the whole convection system was toward the transformation into a characteristic bow echo structure, which was reached at 19:20 UTC and lasted beyond this time. Such a development phase of the considered MCS is presented in Fig. 29.

After a temporary decrease, there was a sharp increase in electric activity and propagation speed of the MCS, as shown in Fig. 15 at 19:10 UTC. Moreover, as the surface wind records reported by Mańczak et al. (2021) and Wrona et al. (2022) have shown, also the strength of surface wind activity increased rapidly and, at the time period of the derecho, it entered into the most destructive force. At the beginning of this development period, at 19:10 UTC, the developing bow echo MCS structure consisted of four distinct and separated thunderstorm areas presented clearly in Fig. 28. In turn, going back to the synchronous courses of the MCS

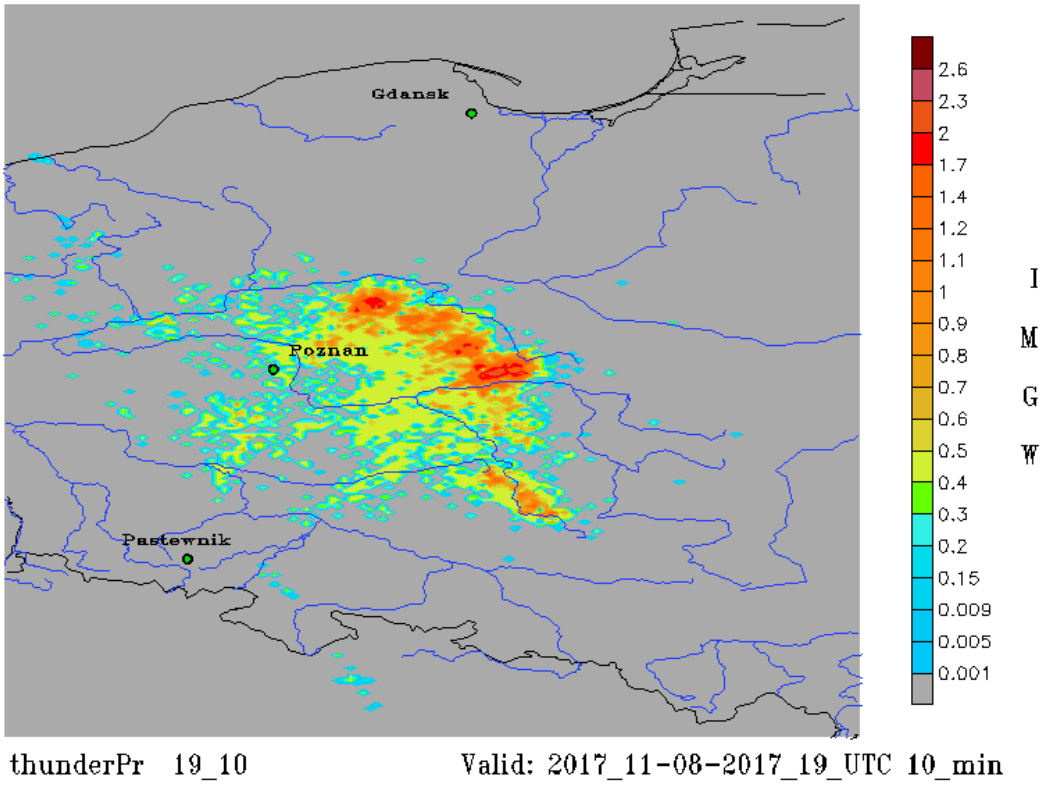

Fig. 28. Characteristic bow echo structure of the considered MCS that was indicated at 19:10 UTC and given by the relevant values of VFS number according to the colored bar on the right. Three green circles stand for the Pastewnik, Poznań, and Gdańsk radar location, respectively.

propagation velocity and the MCS electrical activity expressed by VFS number given in Fig. 15, we can notice that the absolute maximum of VFS number of 3.93 was reached at 19:50 UTC, whereas the four-chamber convective structure was transformed into three massive thunderstorm centers to merge 20 minutes later, at 19:30 UTC, as the expanded and arched thunderstorm structure presented in Fig. 29. Such state lasted until 20:10 UTC. After this time, we have noticed the process of the torn and splitting of the western part of the whole convective system described in detail in Section 4 and presented in Figs. 12–13. Such process ended with a clear breakdown of the MCS into two branches, i.e., the first stronger and eastern, and the second weaker and western, which then turned north, as shown in Figs. 11–12 and 29–35. This MCS transformation process evolved further until 20:30 UTC, when it was possible to distinguish two convection regions separated by the Vistula river, i.e., the west part and the east part. By 20:50 UTC, the western convective region was more electrically active, reaching the relevant VFS number equal to 3.44 at 20:40 UTC and equal to 3.10 at 20:50 UTC, as shown in Fig. 29 by the time span from 20:30 to 21:00 UTC and in Fig. 35 by the time span from 21:10 to 21:50 UTC. The whole course of this MCS development phase lasted from 19:00 to 21:00 UTC, which was documented by changes in the relevant value of VFS number obtained from the real time PERUN lightning detection data and presented in Fig. 29, as a sequence of the selected seven maps given with the 20-minute time step.

The supplementary synoptic context of the MCS development process lasting from 17:30 to 21:00 UTC was presented in Figs. 30–33 by four simulated maps of the relevant parameters (teta), *RoV*, *Rot*, and PT_{Ri} obtained at 20:45 UTC, i.e., at the simulation output time close to the time moment of the MCS split incident determined from the PERUN lightning detection data.

Additionally, after Łapeta et al. (2021), the METEOSAT SEVIRI color-enhanced IR rightness temperature image of the considered supercell formation over Poland on 11 August 2017, taken from the EUMETSAT 2017 at 20:45 UTC, was shown in Fig. 34.

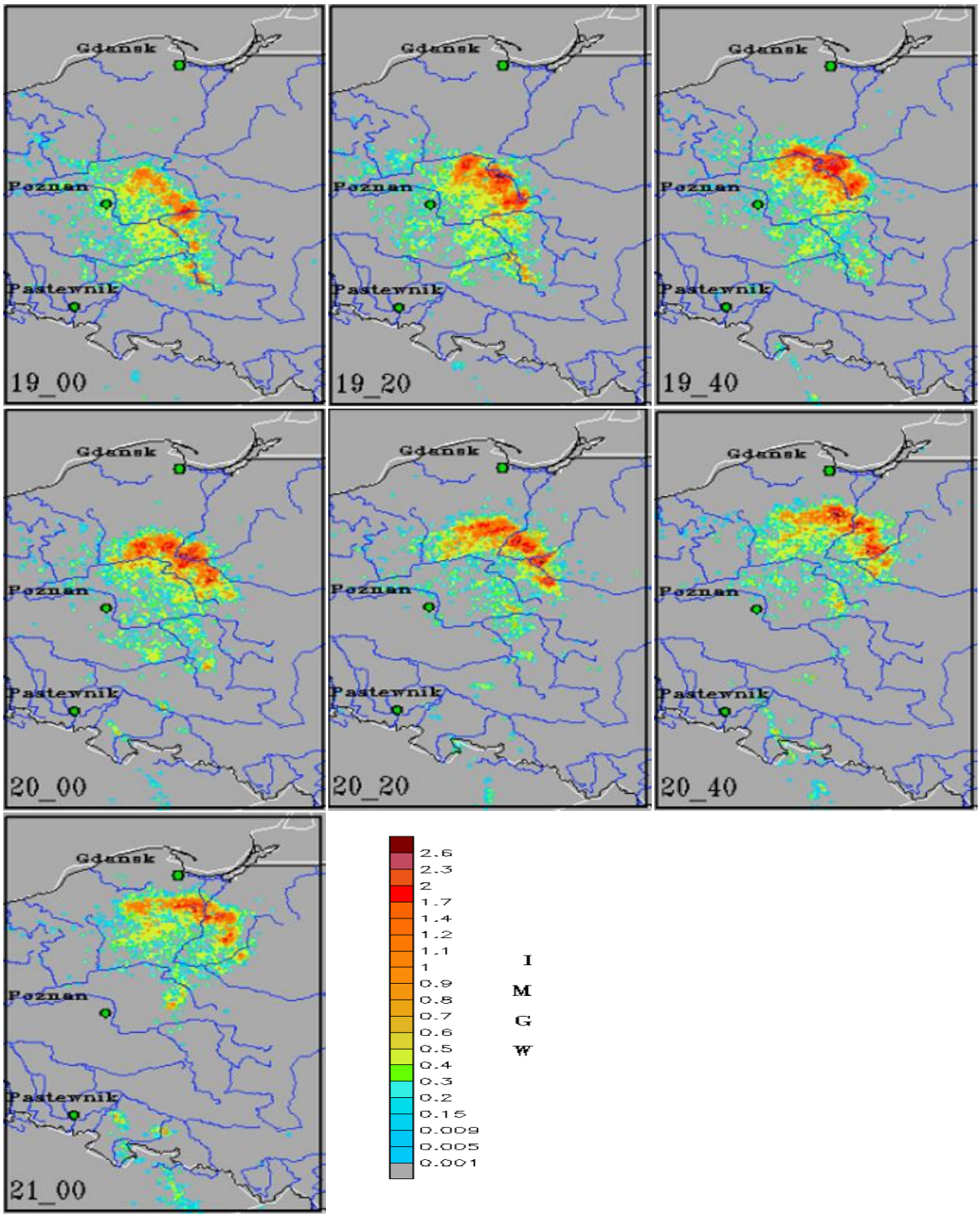

Fig. 29. Time sequence of seven maps given with the 20-minute time step presenting the relevant electrical activity changes during the MCS development stage that lasted from 19:00 to 21:00 UTC.

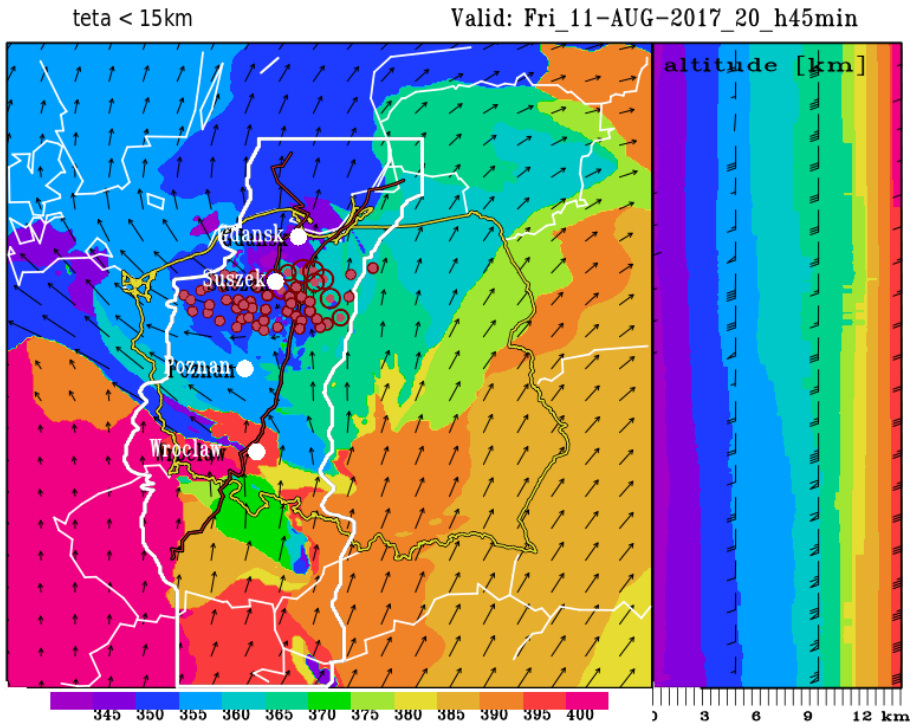

Fig. 30. The same as in Fig. 18, but showing the pattern for the simulated map of the (teta) parameter and lightning activity calculated at 20:45 UTC.

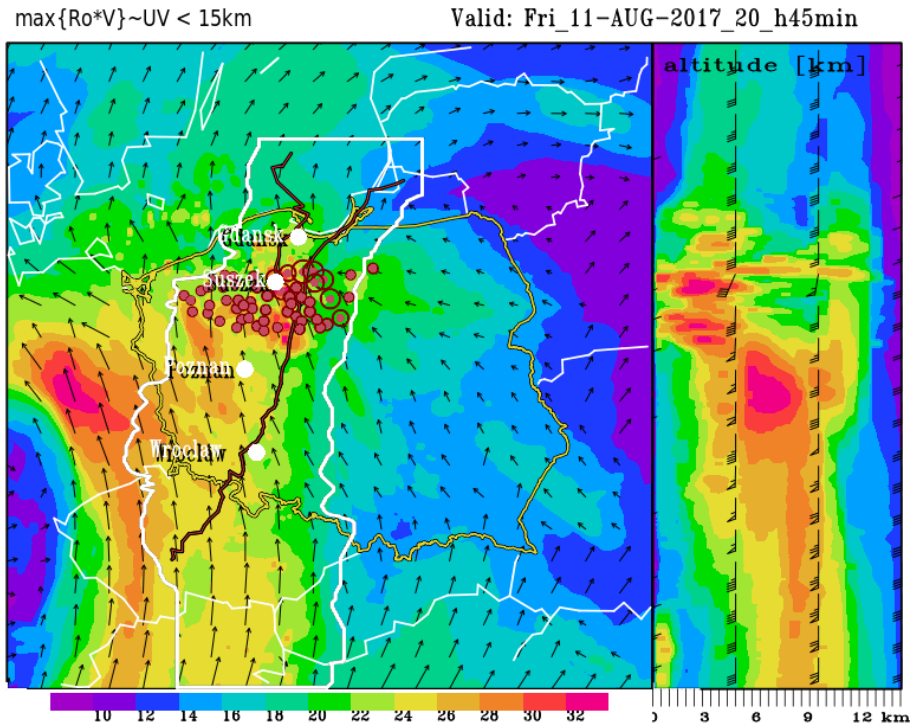

Fig. 31. The same as in Fig. 30, but showing the pattern for the simulated map of the *RoV* parameter and lightning activity calculated at 20:45 UTC.

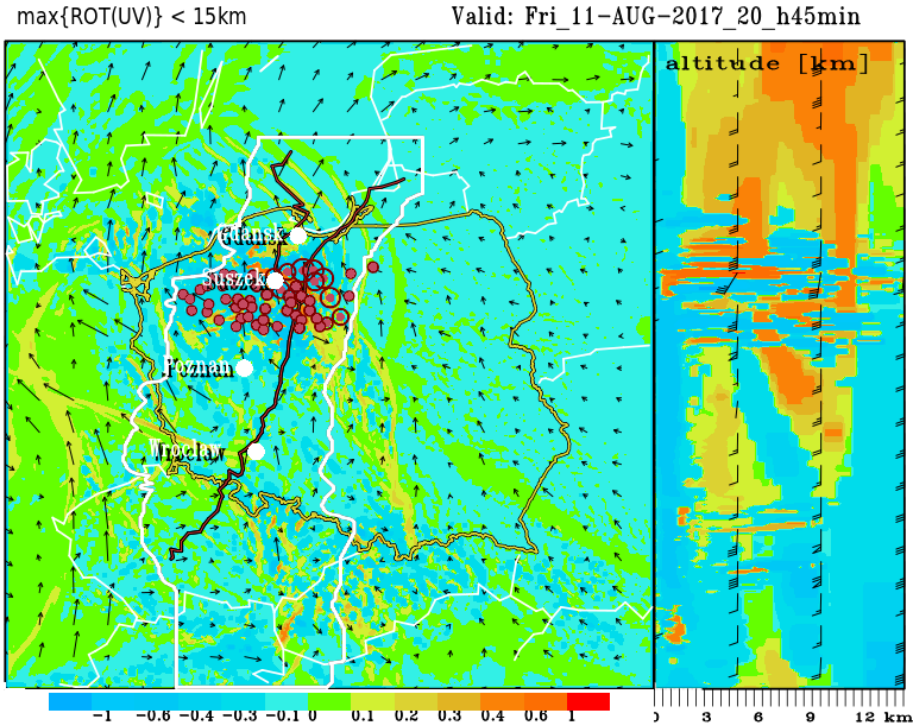

Fig. 32. The same as in Fig. 30, but showing the pattern for the simulated map of the *Rot* parameter and lightning activity calculated at 20:45 UTC.

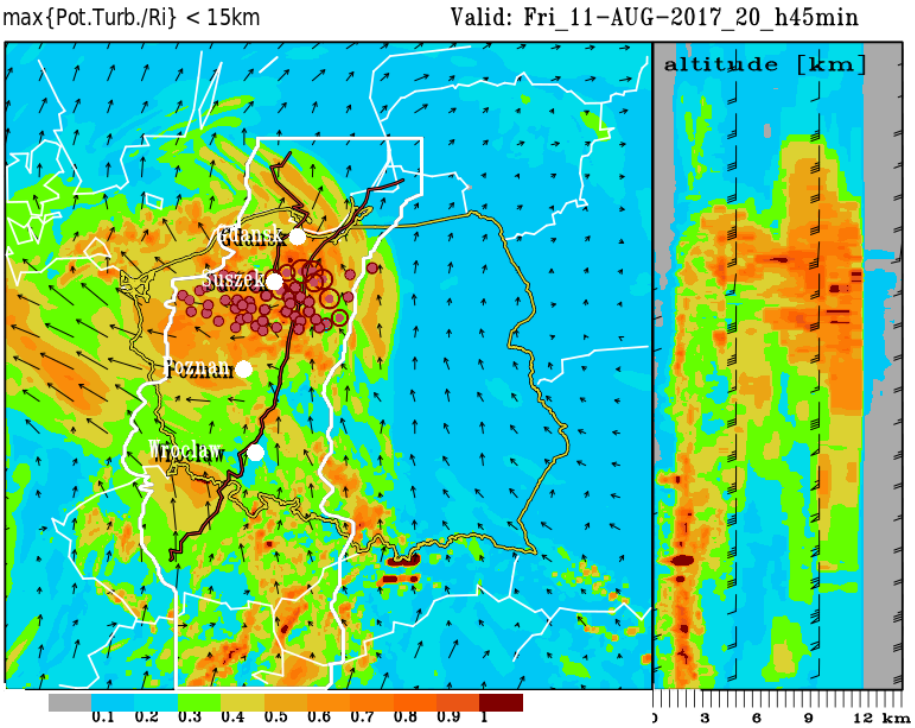

Fig. 33. The same as in Fig. 30, but showing the pattern for the simulated map of the PT_{Ri} parameter and lightning activity calculated at 20:45 UTC.

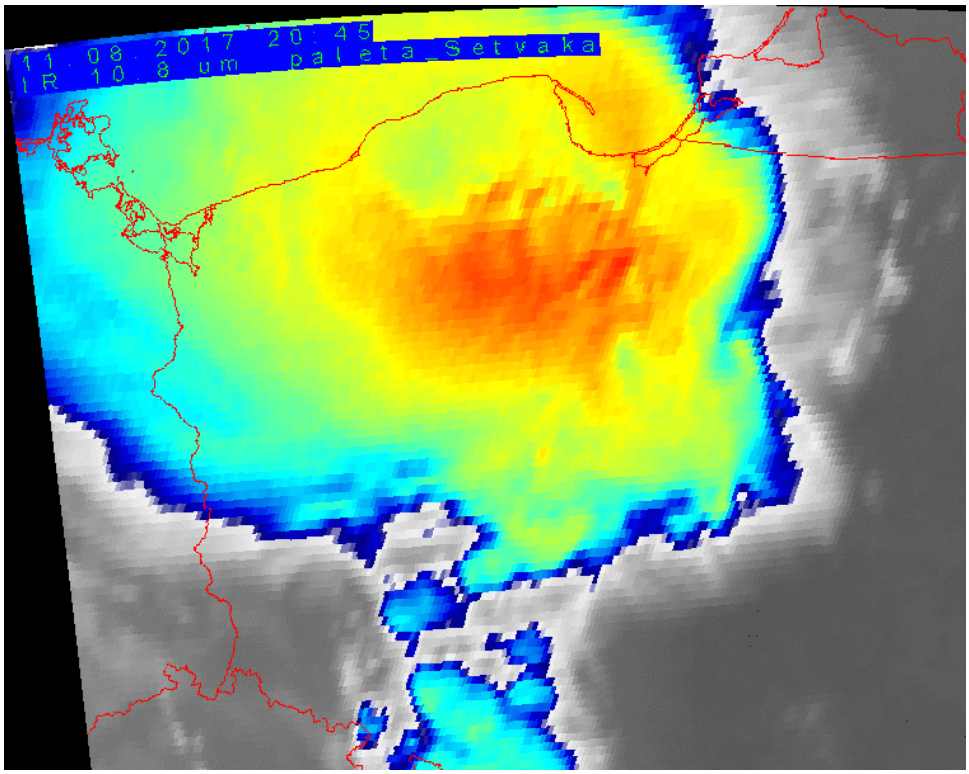

Fig. 34. METEOSAT SEVIRI color-enhanced IR brightness temperature image of the considered supercell formation over Poland on 11 August 2017 taken at 20:45 UTC (© EUMETSAT 2017, © dane.sat4envi.imgw.pl, © OpenStreetMap contributors, reported also by Łapeta et al. (2021)).

Bearing in mind that the MCS spilt incident was a characteristic feature of the convective process during this MCS development, we can find that a separate thunderstorm area occurred in the Suszek region between 20:00 and 21:00 UTC and retained its subjectivity/coherence in the northward movement. It meant a creation, detachment, or just a split of the MCS path, whatever we call it, and a new-line MCS movement was detached from its previous main track as a side track of the appearing derecho episode. At first, as it was shown in Fig. 30, the tropopause is evidently lowered over the derecho track, with the maximum depression preceding the MCS position, and at 20:45 it is located north of Suszek. After the MCS passage, i.e., south of Suszek, clearly higher tropopause temperatures prevail. The wind field simulated at the moment at an altitude of approx. 12 000 m confirms the separation of the stream into a more western and north-eastern branch. Secondly, as it was shown in Fig. 31, the air momentum stream transferred the kinetic energy from the upper troposphere to the ground layers and its maximum value reached the ground layers just in the Suszek area. Thirdly, as it was presented in Fig. 32, high values of the wind rotation field, alternating positive and negative, coincided well with the supercell space domain, which was clearly seen in the satellite IR images. At this time, the whole MCS determined from the activity of lightning discharges resided in the supercell area. On the other hand, as indicated in Fig. 33, the Richardson component of turbulence potential located the supercell space domain quite well, and similarly to the location provided by the wind rotation field, especially at the sub-tropopausal levels. Taking into account that the satellite diagnostics of the supercell occurrrence, as given by Setvak et al. (2010), is related to the temperature of the upper atmosphere by a cold ring or cold U shape, we can note that such a numerical index PT_{Ri} as depicted in Fig. 33 enables complementary phenomenological diagnostics of supercell formations. In turn, the temperature of supercell top shown by IR brightness image in Fig. 34 uniquely and phenomenologically

diagnoses the supercell space domain. The considered synoptic context that has turned out to be a supercell formation, needs further tracing of the supercell, in space and time, to better understand the whole derecho evolution process. However, some limitations of such phenomenological diagnostics are well illustrated by the quotation taken from Łapeta et al. (2021): "The transformation from cold U shape into a cold ring structure again seemed to begin around 20:30 UTC, however, the temperature distribution along the ring was not homogenous and a distinctive minimum can be seen in its northwestern part. This complicated structure should be considered as the result of the interaction between single overshooting tops located close to each other."

5.4 The final, fourth stage development, from 21:10 to 23:50 UTC, with weakening and degradation of the whole MCS

The final completion of the whole MCS evolution process resulted in the single remnant thunderstorm cluster activity on the western MCS flank, that was departed from the main system at about 20.40 UTC and farther moved north. At first, this part of MCS kept its strength and individuality but later on started to dissolve quickly. At the same time, on the eastern MCS flank, its eastern thunderstorm part was also weakening. Then the main convection areas entered the Vistula river delta and, still weakening, moved northeast towards the Courland. At the same time, the weak convection region of the MCS western flank was taken by its western branch, and then weakened, entering the area of the Gdańsk Bay. Such a final stage of the considered MCS development is presented in Fig. 35 by the time sequence of six maps given with the 20-minute time step.

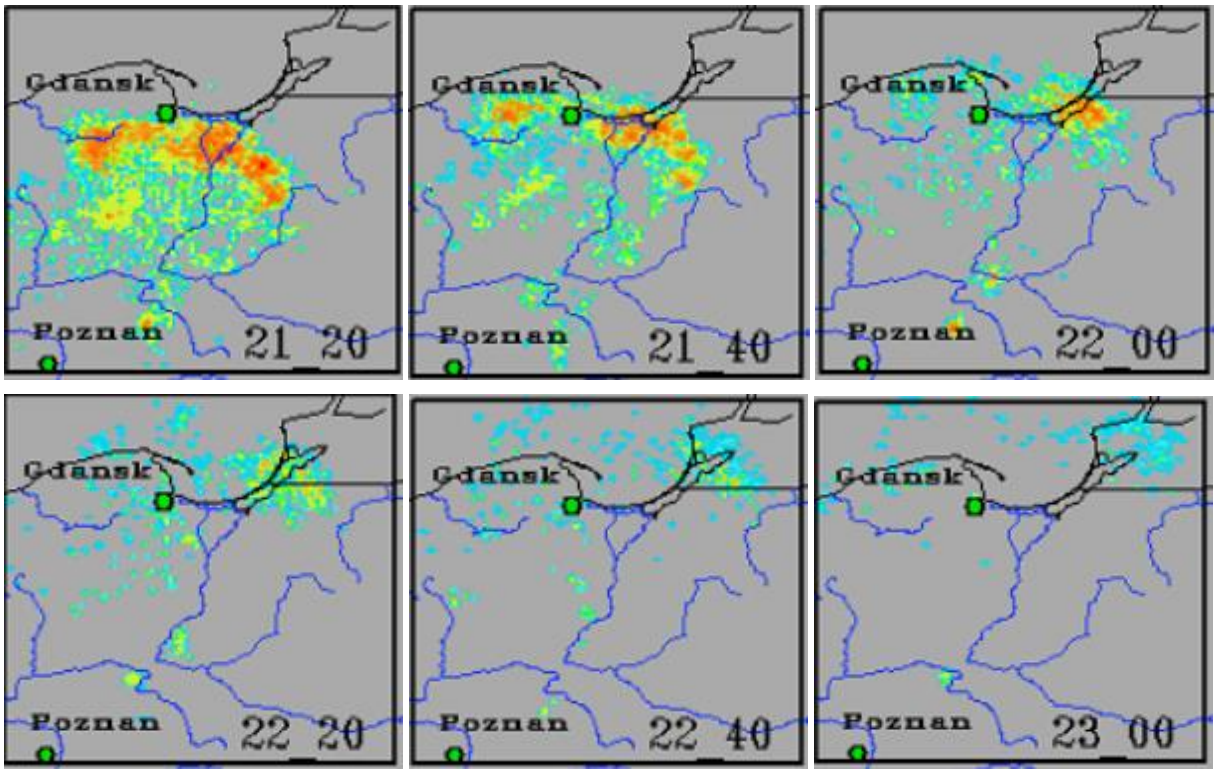

Fig. 35. Time sequence of six maps given with the 20-minute time step, presenting the relevant electrical activity changes during the final MCS development stage that lasted from 21:00 to 23:00 UTC.

The synoptic context of the last MCS development stage with the degradation phase that lasted from 21:10 to 23:50 UTC is presented in Figs. 36–39 by the set of four maps for *p3D*, (teta), *RoV*, and *Rot* parameters simulated at 23:45 UTC together with the adequate 3D wind field taken from the NWP model and lightning discharge detections obtained from the PERUN

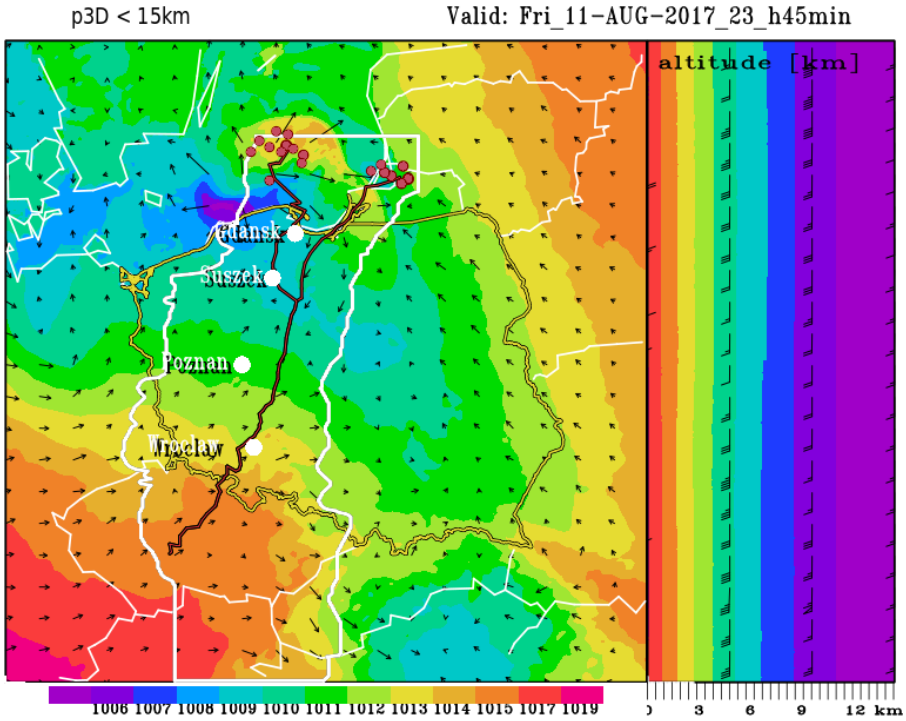

Fig. 36. The same as in Fig. 17, but showing the pattern for the simulated map of the *p3D* parameter and lightning activity calculated at 23:45 UTC.

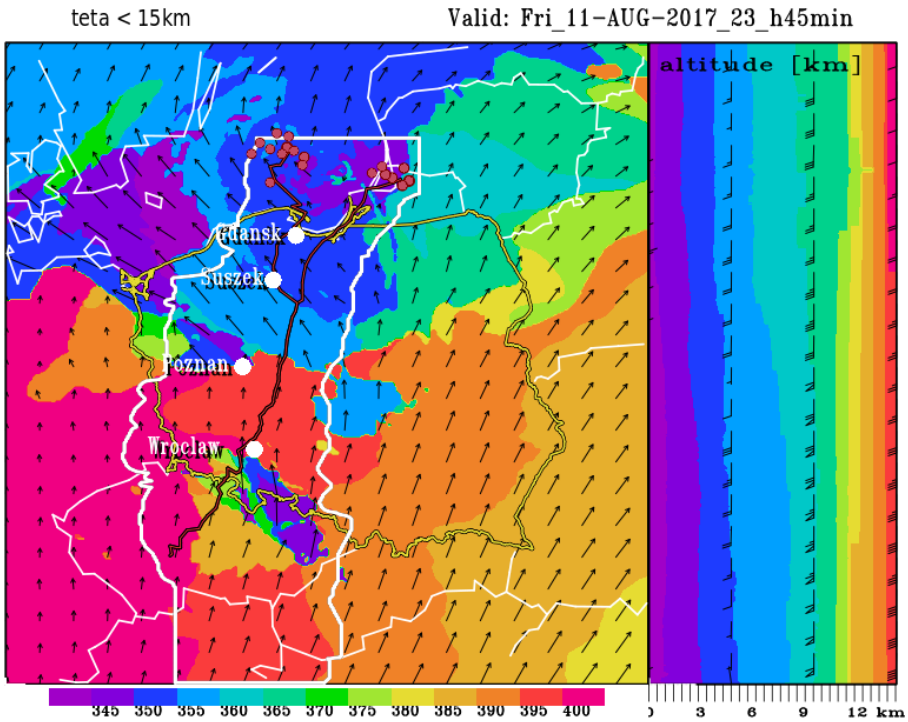

Fig. 37. The same as in Fig. 18, but showing the pattern for the simulated map of the (teta) parameter and lightning activity calculated at 23:45 UTC.

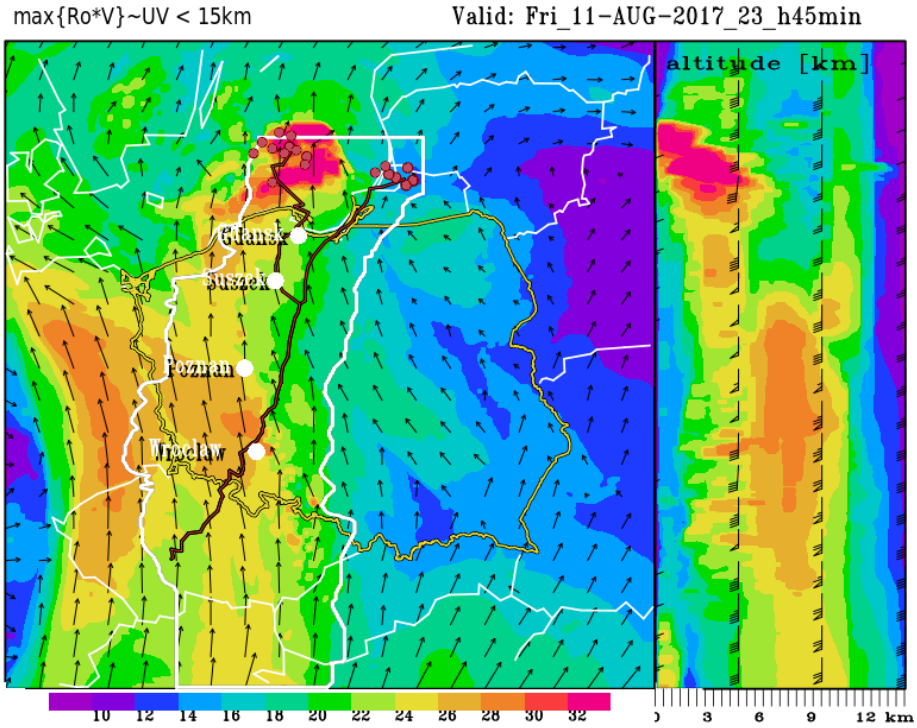

Fig. 38. The same as in Fig. 19, but showing the pattern for the simulated map of the *RoV* parameter and lightning activity calculated at 23:45 UTC.

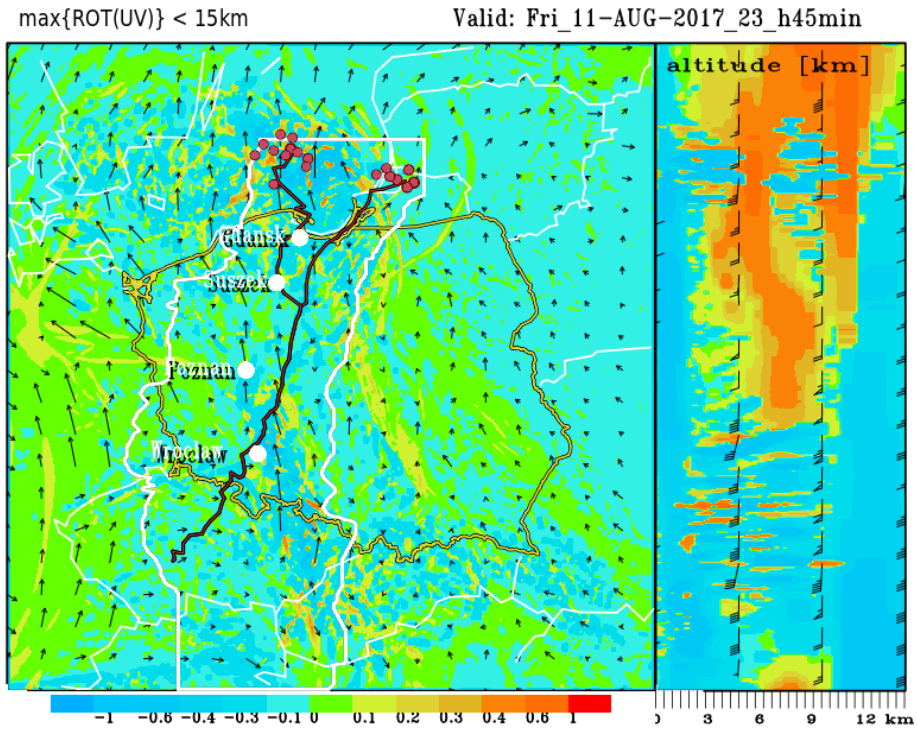

Fig. 39. The same as in Fig. 20, but showing the pattern for the simulated map of the *Rot* parameter and lightning activity calculated at 23:45 UTC.

data. Additionally, the METEOSAT SEVIRI color-enhanced IR brightness temperature image cofirming the final MCS degradation together with its split and taken from the EUMETSAT 2017 database at 23:45 UTC is given in Fig. 40.

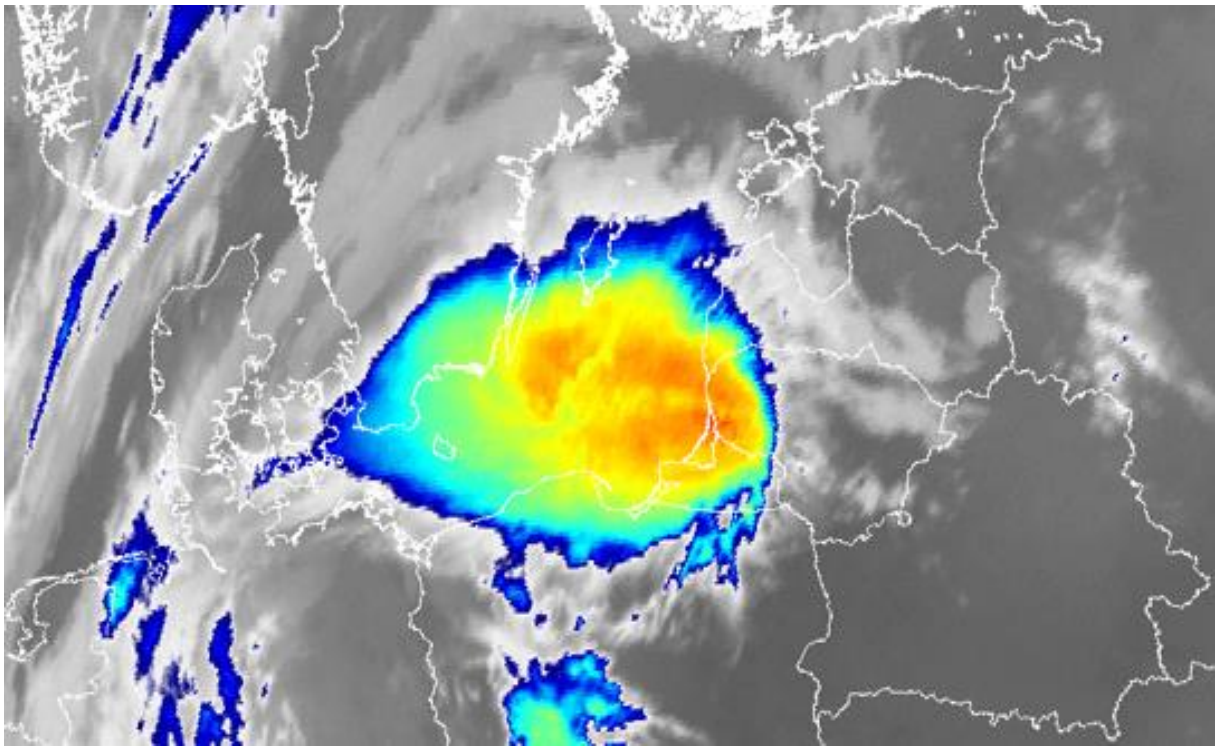

Fig. 40. METEOSAT SEVIRI color-enhanced IR brightness temperature image at 23:45 UTC on 11 August 2017 (© EUMETSAT 2017, © dane.sat4envi.imgw.pl, © OpenStreetMap contributors, reported also by Łapeta et al. (2021)).

A characteristic feature of this process, given in Figs. 35–39, was a distinct weakening and degradation of the whole MCS. As it was shown in Fig. 15, after 22:10 UTC, all VFS values are below 1. It is interesting that in the area of Wrocław at 22:10 UTC new lightning discharges are detected as a replica of a later derecho episode and they move farther north, reaching Poznań. But this lightning discharges zone lies far south of the considered supercell, which lasts itself until the end of the study period, i.e., 00:00 UTC on the next day, 12 August 2017. Its decay will come later.

In turn, as it can be retrieved from Fig. 36, the pressure depression noticeably weakens and decreases in the considered area after 23:15 UTC. Nevertheless, at the ground-level, the wind field pattern is a characteristic peculiarity indicating a strong downburst combined with a horizontal outbreak. Moreover, we can find from Fig. 37 that the tropopause depression still accompanies MCS, including both propagation paths with two characteristic discharge groups, but the area of low potential temperature values has shrunk considerably. On the other hand, based on Fig. 38 it can be noticed that the power to the considered MCS is cut off through the nucleus of the tropospheric jet after 22:45 UTC. However, the maximum of air momentum is concentrated below 3 km, while, after 21:30 UTC, in the vicinity of the western border of Poland, the jet stream is fragmented into a western branch, associated with the mother cyclone from above Germany, and an eastern branch controlling the following derecho episode. However, the whole MCS is weakening but not fading away. Finally, as can be seen in Fig. 39, the negative (anticyclonic) rotation dominates the considered supercell area from 21:30 UTC. In this final evolution phase, at 23:15 UTC, the whole MCS divides definitively into two areas. As for the vertical currents, given by the *W3D* parameter, they remain until the end of the period under study, i.e., until 00:00 UTC of the next day, 12 August 2017, but after 20:45 UTC their

domain shrinks noticeably. The turbulence index PT_{Ri} remains unchanged in area, but its values in the middle troposphere are getting weaker.

6. CONCLUSIONS

According to the evaluation of Parfiniewicz and Konarski (2016), the MCS with the derecho episode over Poland on 11 August 2017, reaching the maximum value of VFS number equal to 3.93, was not a strong convective incident on the European scale. The main MCS propagation path expressed in the coordinates of the COSMO_2.8 km model was abstracted and then used to determine the propagation speed of this convection system. These calculations were performed only for the main MCS propagation path. The highest estimated propagation speed, up to 40 m/s, occurred around 19:30 UTC, preceding the MCS path split. Although the calculated MCS propagation speeds are burdened with some errors, they still remain fairly consistent with the telemetry and damage measurements reported by Mańczak et al. (2021), Wrona et al. (2022), and Taszarek et al. (2019a,b). The basic characteristic parameters, such as the traveled distance, the lifetime, and the average propagation speed of the considered MCS with the derecho event were also estimated. They were equal to 864.42 km, 11.17 hours, and 21.50 m/s, i.e., 77.4 km/h, respectively. Moreover, 24 records of wind gusts exceeding 20 m/s were shown by the telemetry data gathered along the evaluated MCS path. Although those severe wind gusts were noted on both sides of the main MCS track, the wind gusts activity seemed to be dominant on the MCS west side and well correlated with the most spectacular damages reported in the Bory Tucholskie Forest. Certainly, the derecho electrical activity dominated the eastern MCS flank, but for understandable reasons, most of the attention in the papers cited above was focused on the analysis of the western MCS flank,well documented by the radar data from Poznań and Gdańsk. The review and analysis of 144 maps displaying the evolution of MCS electrical activity expressed by changes of the relevant VFS number allowed to describe and present all MCS development stages, including this remarkable episode of the "Suszek" convection incident and other MCS essential details responsible for its electrical activity. It was done in a novelty way which, to our best knowledge, has never been used in any published papers dealing with this case of MCS. Our individual approach to this study complements and well validates other phenomenological evaluations related to the assessment of such severe convection episodes. The considered MCS case of the very fast-moving convective system is significantly different from the cases we have studied earlier and that occurred in Poland, e.g., the stormy day on 28 March 1997 with the hurricane incident on the Baltic Sea analyzed in Parfiniewicz (2001) or the tornado case of 20 July 2007 reported by Parfiniewicz et al. (2009) and Parfiniewicz (2014). No doubt, a better understanding of each MCS case and processes involved in its development requires a separate and detailed diagnosis in different fields, while our paper dealing with this issue is phenomenological in nature and is only a modest contribution to the achievement of such a primary goal. At the end, we should also underline that our idea of the conversion of the primary lightning discharge density field to the presentation of this field by the particular scalar value of the relevant VFS number based on two empirical formulas, given in Section 4 by Eqs. (1)–(2), was successfully implemented to some nowcasting procedures used by the internet portal of awiacja_imgw_pl to indicate – on the background of thunderclouds radar reflectivity – their areas where the vigorous convection development was anticipated, posing a danger for people, different objects of ground infrastructure, or even for plane communication.

Acknowledgments. We express our gratitude to Dr. Michał Ziemiański, expert in meteorology, for his effective, meaningful, and creative support. Many thanks to Mrs. Marzena Kawecka and prof. Jan Szturc for the rainfall data from the INKA system, and also to Anna

Goławska for providing valuable supplementary telemetry data. To Jerzy Konarski and Wojciech Gajda for PERUN data and to Wiesław Łazarewicz and Jan Walasek for joint works on nowcasting thunderstorms for https://awiacja.imgw.pl/. We also thank the reviewers for their insightful comments and valuable advice. Chapter 5 of this work, devoted to the evolution of the MCS on a synoptic background, was made on the computing infrastructure of the Interdisciplinary Centre for Mathematical and Computational Modelling (ICM) of the University of Warsaw under the Allocation No. G88-1220: "Suszek".

References

Barański, P., and J. Parfiniewicz (2019), The derecho episode in the Bory Tucholskie district 11 August 2017 – the present state of the predicting severe storms by awiacja_imgw_pl. **In:** *Proc. 10th European Conference on Severe Storms, 4–8 November 2019, Kraków, Poland*, ECSS2019-6-2, DOI: 10.13140/RG.2.2.19737.36965.

Bodzak, P., Z. Dziewit, and W. Gajda (2006), The ratio of cloud to cloud-to-ground flashes in summer seasons for Poland territory on the basis of data from PERUN system. **In:** *Proc. 19th International Lightning Detection Conference, 24–25 April 2006, Tucson, USA*.

Celiński-Mysław, D., and D. Matuszko (2014), An analysis of selected cases of derecho in Poland, *Atmos. Res.* **149**, 263–281, DOI: 10.1016/j.atmosres.2014.06.016.

Fujita, T.T. (1978), Manual of downburst identification for project NIMROD, Satellite and Mesometeorology Research Project, The University of Chicago, Research Paper No. 156, 104 pp.

Lelątko, I. (2020), Ekstremalnie silne porywy wiatru 11 sierpnia 2017. Wstępna analiza przypadku z punktu widzenia pracy operacyjnej IMWM–NRI CBPM Kraków, available from: http://intranet.imgw.ad/wp-content/uploads/2020/11/BowEchoOf 11 August 2017Iwona.pdf (in Polish).

Łapeta, B., E. Kuligowska, P. Murzyn, and P. Struzik (2021), Monitoring the 11 August 2017 storm in central Poland with satellite data and products, *Meteorol. Hydrol. Water Manage.*, DOI: 10.26491/mhwm/144590.

Łuszczewski, H., and I. Tuszyńska (2022), Derecho radar analysis of August 11, 2017, *Meteorol. Hydrol. Water Manage.*, DOI: 10.26491/mhwm/152504.

Mańczak, P., B. Wrona, A. Woźniak, M. Ogrodnik, and M. Folwarski (2021), Synoptic analysis of derecho over Poland on 11 July 2017, *Meteorol. Hydrol. Water Manage.* (submitted).

Marshall, J.S., and W. Mc K. Palmer (1948), The distribution of raindrops with size, *J. Meteorol.* **5**, 4, 165–166, DOI: 10.1175/1520-0469(1948)005 <0165:TDORWS>2.0.CO;2.

Mazur, A., G. Duniec, W. Interewicz, and A. Wyszogrodzki (2019), Ensemble forecasting of extreme convective phenomena using universal tornadic index. **In:** *Proc. 10th European Conference on Severe Storms, 4–8 November 2019, Kraków, Poland*, ECSS2019-57.

Parfiniewicz, J.W. (2001), Addendum to "Diagnostic study – storm over Poland", *Meteorol. Z.* **10**, 2, 151–152, DOI: 10.1127/0941-2948/2001/0010-0151.

Parfiniewicz, J. (2012), Concerning Thunderstorm Potential prediction. **In:** *The European Meteorological Society Annual Meeting Abstracts*, Vol. 9, No. EMS2012-81, 12th EMS / 9th ECAC, available from: http://meetingorganizer.copernicus.org/EMS2012/EMS2012-81.pdf.

Parfiniewicz, J. (2013), Nowcasting strong convective events (SCE) – the thunderstorm thermometer. **In:** *Meteorological Technology World Expo 2013 Preview*, available from: http://www.ukintpressconferences.com/uploads/SPMTWX13/Breakout_Session_d2_s2_p5_Jan_Parfiniewicz.pdf; http://viewer.zmags.com/publication/f088b3fc#/f088b3fc/62.

Parfiniewicz, J. (2014), Steps to a storm – forecasting and nowcasting strong convective events, *Meteorol. Technol. Int.* **April 2014**, 48–51, available from: http://viewer.zmags.com/publication/c4f984ab#/c4f984ab/50.

Parfiniewicz, J., and P. Barański (2014), An explosive convection over Europe with 8-minute tornado incident in Poland on July 20, 2007, *Int. J. Environ. Eng. Nat. Resour*. **1**, 6, 262–276.

Parfiniewicz, J., and G. Bojanek (2013), Jak możemy pomóc w weryfikacji prognoz turbulencji CAT? Dlapilota.pl, Prognozowanie Clear Air Turbulence, available from: http://dlapilota.pl/wiadomosci/dlapilota/jak-mozemy-pomoc-w-weryfikacji-prognoz-turbulencji-cat (accessed: 21 November 2013) (in Polish).

Parfiniewicz, J., and J. Konarski (2016), On thunderstorm quantification (continuation), *COSMO Newslett*. **16**, 13–15, DOI: 10.13140/rg.2.2.29118.08007.

Parfiniewicz, J., P. Barański, and W. Gajda (2009), Preliminary analysis of dynamic evolution and lightning activity associated with supercell event: case story of the severe storm with tornado and two heavy hail gushes in Poland on 20 July 2007, *Publs. Inst. Geoph. PAS* **D-73 (412)**, 65–88.

Richard, P., and J.Y. Lojou (1996), Assessment of application of storm cell electrical activity monitoring to intense precipitation forecast. **In:** *Proceedings: 10th International Conference on Atmospheric Electricity, June 10–14, 1996*, International Commission of Atmospheric Electricity, Osaka, Japan, 284–287.

Setvák, M., D.T. Lindsey, P. Novák, P.K. Wang, M. Radová, J. Kerkmann, L. Grasso, S.-H. Su, R.M. Rabin, J. Štástka, and Z. Charvát (2010), Satellite-observed cold-ring-shaped features atop deep convective clouds, *Atmos. Res.* **97**, 1–2, 80–96, DOI: 10.1016/j.atmosres.2010.03.009.

Szturc, J., A. Jurczyk, K. Ośródka, A. Wyszogrodzki, and M. Giszterowicz (2018), Precipitation estimation and nowcasting at IMGW-PIB (SEiNO system), *Meteorol. Hydrol. Water Manage.* **6**, 1, 3–12, DOI: 10.26491/mhwm/76120.

Taszarek, M., N. Pilguj, J. Orlikowski, A. Surowiecki, S. Walczakiewicz, W. Pilorz, K. Piasecki, Ł. Pajurek, and M. Półrolniczak (2019a), Derecho evolving from a mesocyclone—a study of 11 August 2017 severe weather outbreak in Poland: event analysis and high-resolution simulation, *Mon. Wea. Rev*. **147**, 6, 2283–2306, DOI: 10.1175/MWR-D-18-0330.1.

Taszarek, M., N. Pilguj, J. Orlikowski, A. Surowiecki, S. Walczakiewicz, W. Pilorz, K. Piasecki, Ł. Pajurek, and M. Półrolniczak (2019b), Derecho evolving from a mesocyclone—a study of 11 August 2017 severe weather outbreak in Poland: event analysis and high-resolution simulation, ECSS2019-77, 4–8 November 2019, Kraków, Poland.

Wrona, B., P. Mańczak, A. Woźniak, M. Ogrodnik, and M. Folwarski (2022), Synoptic conditions of the derecho storm. Case study of the derecho event over Poland on August 11, 2017, *Meteorol. Hydrol. Water Manage.*, DOI: 10.26491/mhwm/152798.

Received 16 September 2022
Received in revised form 30 December 2022
Accepted 31 December 2022